Department of Micro- and Nanosciences

Theoretical studies of optical transitions in semiconductor quantum structures

Osmo Vänskä

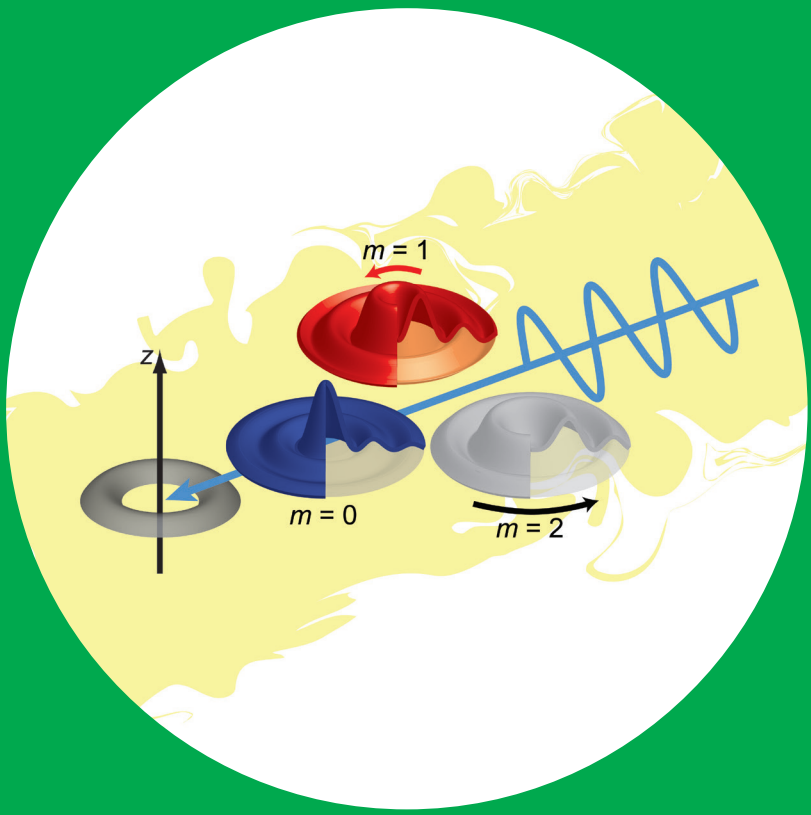

Aalto University

DOCTORAL DISSERTATIONS

Aalto University publication series
DOCTORAL DISSERTATIONS 214/2014

Theoretical studies of optical transitions in semiconductor quantum structures

Osmo Vänskä

A doctoral dissertation completed for the degree of Doctor of Science (Philosophy) to be defended, with the permission of the Aalto University School of Electrical Engineering, at a public examination held at the lecture hall TU1 of the TUAS building (Otaniementie 17, Espoo, Finland) on the 9th of January 2015 at 12 noon.

Aalto University
School of Electrical Engineering
Department of Micro- and Nanosciences
Micro and Quantum Systems Group

Supervising professor
Prof. Ilkka Tittonen

Thesis advisor
Prof. Mackillo Kira, Philipps-Universität Marburg, Germany

Preliminary examiners
Prof. Markus Lindberg, Åbo Akademi University, Finland
Prof. Frank Jahnke, University of Bremen, Germany

Opponent
Prof. Antti-Pekka Jauho, Technical University of Denmark, Denmark

Aalto University publication series
DOCTORAL DISSERTATIONS 214/2014

ISBN 978-952-60-6032-3 (printed)
ISBN 978-952-60-6033-0 (pdf)
ISSN-L 1799-4934
ISSN 1799-4934 (printed)
ISSN 1799-4942 (pdf)
http://urn.fi/URN:ISBN:978-952-60-6033-0

Unigrafia Oy
Helsinki 2014

Finland

441 697
Printed matter

Aalto University

Abstract

Aalto University, P.O. Box 11000, FI-00076 Aalto www.aalto.fi

Author
Osmo Vänskä

Name of the doctoral dissertation
Theoretical studies of optical transitions in semiconductor quantum structures

Publisher School of Electrical Engineering

Unit Department of Micro- and Nanosciences

Series Aalto University publication series DOCTORAL DISSERTATIONS 214/2014

Field of research Electrophysics

Manuscript submitted 19 August 2014 **Date of the defence** 9 January 2015

Permission to publish granted (date) 21 October 2014 **Language** English

☐ **Monograph** ☒ **Article dissertation (summary + original articles)**

Abstract

Nanotechnologically fabricated structures out of compound semiconductor materials make up the functional parts in LEDs, in semiconductor lasers and in electronics components. The small size of the structures evidently leads to requiring the modeling to look at phenomena at the quantum level. Especially for optoelectronical devices, one needs to treat the interaction between light and semiconductor material. This research adds to the understanding of interpretations of light-matter interaction phenomena and makes it possible to find totally new and undiscovered functionalities in semiconductor nanostructures.

This thesis presents work on modeling and creates new theoretical foundations for phenomena appearing in semiconductor quantum structures. Of special interest has been to generate a theoretical description to such phenomena that have been caused by an optical field and in which one sees changes, e.g., in angular momentum or spatial distribution of excited states. Basically, two kinds of structures are examined, quantum rings and wells. A quantum ring is a toroidal object of which volume is very small, but its diameter can be significant when compared to the wavelength of light. Another class of systems under study is a double quantum well structure, where there are two quantum wells on both sides of a tunnel barrier. In this system, the type-I and type-II semiconductor band-structure properties become combined in spatial coordinates, since the electrons and holes can occupy either the same or the separate quantum wells.

The two most interesting results are the angle-of-emission dependent photoluminescence from the quantum rings and the coherent control of vertical transport of desired quasiparticles through material interfaces in the quantum-well system in a selective manner. Since the obtained results on quantum rings are closely connected to the orbital-angular-momentum coupling between light and matter, they can prove to be important in different quantum information schemes where this angular-momentum aspect of light has been found to be highly beneficial. In quantum optics, there already are visible trends towards this direction. The predicted coherent control in a double-quantum-well system may mean a large technological progress, since by utilizing this effect one can study transport properties between materials over an interface, one of the most interesting examples of such phenomena being the transfer of quantum correlations through the interface without changing the local densities of electrons.

Keywords semiconductor quantum structures, optical transitions, quantum ring, double quantum well, orbital angular momentum of light, semiconductor quantum optics, coherent control

ISBN (printed) 978-952-60-6032-3 **ISBN (pdf)** 978-952-60-6033-0

ISSN-L 1799-4934 **ISSN (printed)** 1799-4934 **ISSN (pdf)** 1799-4942

Location of publisher Helsinki **Location of printing** Helsinki **Year** 2014

Pages 124 **urn** http://urn.fi/URN:ISBN:978-952-60-6033-0

Aalto-yliopisto

Tiivistelmä

Aalto-yliopisto, PL 11000, 00076 Aalto www.aalto.fi

Tekijä
Osmo Vänskä

Väitöskirjan nimi
Teoreettisia tarkasteluja puolijohteiden kvanttirakenteiden optisista transitioista

Julkaisija Sähkötekniikan korkeakoulu

Yksikkö Mikro- ja nanotekniikan laitos

Sarja Aalto University publication series DOCTORAL DISSERTATIONS 214/2014

Tutkimusala Sähköfysiikka

Käsikirjoituksen pvm 19.08.2014 **Väitöspäivä** 09.01.2015

Julkaisuluvan myöntämispäivä 21.10.2014 **Kieli** Englanti

☐ **Monografia** ☒ **Yhdistelmäväitöskirja (yhteenveto-osa + erillisartikkelit)**

Tiivistelmä

Puolijohdemateriaaleista valmistetut nanorakenteet ovat funktionaalinen osa ledeissä, puolijohdelasereissa ja elektroniikan komponenteissa. Rakenteiden pieni koko johtaa väistämättä siihen, että toiminnallisuuden mallintaminen ja ymmärtäminen edellyttää kvanttimaailman ilmiöiden tarkastelua. Optoelektronisten laitteiden teoreettisen tutkimuksen kannalta tämä tarkoittaa valon ja puolijohdemateriaalin välisen vuorovaikutuksen tutkimista. Tämä tutkimus lisää tietämystä siitä kuinka valo ja materia vuorovaikuttavat keskenään sekä mahdollistaa täysin uusien toiminnallisuuksien löytämisen.

Väitöskirjassa luodaan uutta pohjaa kvanttirakenteissa esiintyvien ilmiöiden selittämiseen. Mielenkiinnon kohteena on ollut generoida teoreettinen kuvaus sellaisille optisen kentän aiheuttamille ilmiöille, joissa puolijohteiden viritystiloissa nähdään muutoksia esimerkiksi liikemäärässä tai spatiaalisessa jakaumassa. Työssä tarkastellaan kahta rakennetyyppiä, kvanttirenkaita ja -kaivoja. Kvanttirengas on toroidin muotoinen objekti, joka on tilavuudeltaan hyvin pieni. Toinen tarkasteltava systeemi on kaksoiskaivorakenne, jossa tyypillisen kvanttikaivon sijasta onkin kaksi kaivoa yhden tunnelointikerroksen eri puolilla. Jälkimmäisessä rakenteessa yhdistyvät tyypin I ja tyypin II puolijohdeominaisuudet paikka-avaruudessa, jossa elektronit ja aukot voivat olla joko samassa tai vaihtoehtoisesti eri kaivossa.

Tärkeimmät tulokset ovat kvanttirenkaiden tapauksessa löydetty valon emissiokulmasta riippuva fotoluminesenssi sekä kaksoiskaivorakenteen yhteydessä ennustettu eri kvasihiukkasten paikan koherentti kontrollointi selektiivisesti. Koska tulokset kvanttirenkaiden osalta ovat kiinteästi yhteydessä ratakulmaliikemäärän vaihtoon sähkömagneettisen kentän ja puolijohteen kvanttitilojen välillä, voivat saavutetut tulokset osoittautua merkittäviksi kvantti-informaatioteknologian eri osa-alueilla. Tämäntyyppisestä trendistä on paljon viitteitä kvanttioptiikan alalla. Kaivorakenteessa löydetty kvasihiukkasten kontrollointi saattaa merkitä suurta teknologista edistysaskelta, sillä hyödyntämällä tätä efektiä voidaan tutkia kulkeutumisprosesseja eri materiaalien välillä, joista erityisen mielenkiintoinen esimerkki on sellainen ilmiö, jossa kvanttikorrelaatiot siirtyvät rajapinnan yli vaikuttamatta hiukkasten sijaintiin.

Avainsanat puolijohteiden kvanttirakenteet, optiset transitiot, kvanttirengas, kaksoiskvanttikaivo, valon ratakulmaliikemäärä, puolijohdekvanttioptiikka, koherentti kontrollointi

ISBN (painettu) 978-952-60-6032-3 **ISBN (pdf)** 978-952-60-6033-0

ISSN-L 1799-4934 **ISSN (painettu)** 1799-4934 **ISSN (pdf)** 1799-4942

Julkaisupaikka Helsinki **Painopaikka** Helsinki **Vuosi** 2014

Sivumäärä 124 **urn** http://urn.fi/URN:ISBN:978-952-60-6033-0

Preface

This thesis is based on the research carried out as a graduate student in the Micro and Quantum Systems group of the Department of Micro- and Nanosciences at Aalto University. Another important place for my research work, which lead to this thesis, has also been the German university town of Marburg. Over the past years, I have had the opportunity to visit Marburg and increase my knowledge of theoretical semiconductor physics. From the same town, I even found the possibility to continue my academic work.

First of all, I wish to express my gratefulness to Prof. Ilkka Tittonen who has given me the possibility to work in science and supervised me. He has compassionately found understanding towards my problems, starting from the smallest and most meaningless up to the most severe ones. Another person who had a crucial role during my doctoral work is Prof. Mackillo Kira who acted as my co-supervisor. Without him this thesis would not exist or at least it would be completely different. I would also like to thank Prof. Stephan W. Koch for his efforts, especially for helping me to better understand the nature of excitons.

I thank Dr. Thomas Lindvall, Dr. Andriy Shevchenko and Julius Nieminen for many interesting discussions about mathematics, physics and the fundamental properties of light. In addition, I am grateful to Dr. Mikhail Erdmanis, Dr. Nikolai Chekurov and Ville Pale. They have faced most of my questions about more practical aspects of nanotechnology and optics, related to the possibilities to experimentally verify my theoretical predictions. I also want to thank all other present and former members of the Micro and Quantum Systems group, including Dr. Päivi Sievilä, Mikko Ruoho and Dr. Ossi Kimmelma.

I acknowledge my funding sources: Teknillisen korkeakoulun tukisäätiö, The National Doctoral Programme in Nanoscience (NGS-NANO), Deutsche

Forschungsgemeinschaft (SFB 1083) and Academy of Finland projects (13140009 and 129043). In addition, I acknowledge Euramet SIB04 project. The EMRP is jointly funded by the EMRP participating countries within EURAMET and the European Union.

Finally, I want to thank my family (Marika, Aino, Alma and Juho), parents and parents-in-law, especially my wife Marika, for their irreplaceable love, support and encouragement.

Marburg, December 14, 2014,

Osmo Vänskä

Contents

List of Publications

This thesis consists of an overview and of the following publications which are referred to in the text by their Roman numerals.

I O. Vänskä, M. Kira, S. W. Koch, and I. Tittonen. Analytical solutions for electronic states in three-dimensional semiconductor quantum rings. *Physica Status Solidi C*, **10**, 1246, June 2013.

II O. Vänskä, M. Kira, I. Tittonen, and S. W. Koch. Indirect interband optical transitions in a semiconductor quantum ring with submicrometer dimensions. *Physical Review B*, **84**, 165317, October 2011.

III O. Vänskä, J. Nieminen, M. Kira, S. W. Koch, and I. Tittonen. Structure-independent semiconductor luminescence equations for quantum rings. *Physica Scripta*, **T160**, 014044, April 2014.

IV J. V. Nieminen, O. Vänskä, I. Tittonen, S. W. Koch, and M. Kira. Accessing orbital angular momentum of quantum-ring excitons via directional semiconductor luminescence. *submitted to a peer-reviewed journal*, October 2014.

V O. Vänskä, I. Tittonen, S. W. Koch, and M. Kira. Coherent terahertz control of vertical transport in semiconductor heterostructures. *submitted to a peer-reviewed journal*, June 2014.

VI M. Erdmanis, L. Karvonen, A. Säynätjoki, X. Tu, T. Y. Liow, Q. G. Lo, O. Vänskä, S. Honkanen, and I. Tittonen. Towards broad-bandwidth polarization-independent nanostrip waveguide ring resonators. *Optics Express*, **21**, 9974, April 2013.

Author's Contribution

Publication I: "Analytical solutions for electronic states in three-dimensional semiconductor quantum rings"

The author contributed the main parts of the original ideas and their conceptualization. All the theoretical and numerical calculations were made by the author. He had a major role in the manuscript preparation process.

Publication II: "Indirect interband optical transitions in a semiconductor quantum ring with submicrometer dimensions"

The author had an important role in conceptualizing the central ideas. He performed all the theoretical and the numerical calculations. As the first author of this article, he drafted the first version of the manuscript and coordinated the writing process.

Publication III: "Structure-independent semiconductor luminescence equations for quantum rings"

Most of the original ideas and their conceptualization were contributed by the author. He performed the major parts of the analytical and numerical calculations. The manuscript of the article is mainly prepared by him.

Publication IV: "Accessing orbital angular momentum of quantum-ring excitons via directional semiconductor luminescence"

The original ideas and conceptualization are mostly done by the author. He contributed to the analytical and numerical calculations as well as to the preparation of the manuscript.

Publication V: "Coherent terahertz control of vertical transport in semiconductor heterostructures"

Together with the Marburg collaborators, the author conceptualized the idea of vertical transport with THz fields. He performed the calculations and designed the used structure. The author prepared the first version of the manuscript and coordinated the following writing process.

Publication VI: "Towards broad-bandwidth polarization-independent nanostrip waveguide ring resonators"

The author contributed to the analytical and numerical results on studied systems and also to the manuscript preparation.

List of abbreviations

3-D	Three dimensional
BBGKY	Bogoliubov-Born-Green-Kirkwood-Yvon
CME	Coulomb matrix element
DME	Dipole matrix element
OAM	Orbital angular momentum
PL	Photoluminescence
QD	Quantum dot
QR	Quantum ring
QW	Quantum well
QWI	Quantum wire
SP	Single particle
THz	Terahertz

List of symbols

$\langle \ldots \rangle$	Expectation value
$\langle N \rangle$	N-particle expectation value
∇	3-D del operator
$\nabla_{\parallel}$	In-plane del operator
$\alpha(\theta, \omega)$	Absorption
γ	Dephasing factor
$\Delta\langle \ldots \rangle$	Correlation
$\Delta\langle N \rangle$	N-particle correlation
ΔN_{ν}	Exciton density
$\Delta\mathrm{PL}(\theta, \omega, \gamma)$	Relative PL intensity
ΔR	In-plane thickness of QR
$\varepsilon(\mathbf{r})$	Dielectric function
θ	Propagation angle of light respect to z axis
λ	Band index
ν	Exciton quantum number
ν_e	Plasma transport frequency
ν_X	Exciton transport frequency
$\xi_{\lambda,i}(\mathbf{r})$	Envelope/confinement function
ρ	Radius coordinate in cylindrical coordinate system
φ	Azimuth angle in cylindrical coordinate system

$\phi_{\nu}^{i,i'}$	Component of exciton wave function
$\psi_{\lambda,i}(\mathbf{r})$	Wave function of electronic state
$\omega_{\mathbf{q}}$	Angular frequency of light mode
$a_{\lambda,i}$	Carrier annihilation operator
$a_{\lambda,i}^{\dagger}$	Carrier creation operator
$B_{\mathbf{q}}$	Photon annihilation operator
$B_{\mathbf{q}}^{\dagger}$	Photon creation operator
c	Conduction band
c_0	Vacuum speed of light
D	Index for doublet contribution terms
$\mathcal{D}_{i,i'}^{\lambda}$	THz dipole matrix element respect $\xi_{\lambda,i}(\mathbf{r})$ functions
$d_{\lambda,\lambda'}$	Dipole matrix element respect $w_{\lambda}(\mathbf{r})$ functions
$D_{i,i'}^{\mathbf{q}}$	Dipole matrix element respect $\xi_{\lambda,i}(\mathbf{r})$ functions
E	Functional of expectation value dynamics
e	Euler's number
$\mathbf{E}(\mathbf{r},t)$	Electric field
$\hat{\mathbf{e}}_{\parallel}$	In-plane unit vector
E_0	Intensity of electric field
e_0	Elementary charge
$E_{\lambda,i}$	Single-particle energy
$\mathcal{E}_{\nu}$	Exciton energy
E_g	Band gap
$\mathrm{E}_{\mathbf{q}}$	Vacuum field amplitude
$\hat{\mathbf{e}}_{\mathbf{q}}$	Polarization vector of light mode
$E_{\mathbf{q}}(t)$	Time dependent amplitude term for electric field
$\hat{\mathbf{e}}_z$	Unit vector to z direction

$f_{\lambda,n,m}(\rho)$	ρ-directional confinement function in QRs
$\mathcal{F}_{M,\nu}$	Exciton oscillatory strength
f_i^e	Electron occupation number
$g_{\lambda,n,m}(z)$	z-directional confinement function in QRs
H	System Hamiltonian or height of a quantum ring
h	Hole band
$\hbar$	Reduced Planck constant
H.c.	Hermitian conjugate
$\mathbf{H}(\mathbf{r})$	Magnetic field
H_0	Single-particle Hamiltonian
H_{C}	Coulomb Hamiltonian
H_{D}	Dipole Hamiltonian
$H_{\mathrm{D,class}}$	Dipole Hamiltonian for classical field
$H_{\mathrm{D,quant}}$	Dipole Hamiltonian for quantum field
$H_{\mathrm{D,THz}}$	Dipole Hamiltonian for classical THz field
i	Imaginary unit
i	General 3-D envelope/confinement quantum number
$I_{\mathrm{PL}}(\theta,\omega)$	PL intensity
J	Index for higher than triplet contribution terms
J_m	Bessel function of the first kind
$\mathbf{k}_{\parallel}$	In-plane momentum quantum number
l	z-directional quantum number
M	Center-of-mass OAM quantum number for excitons
m	φ-directional OAM quantum number
$m^*_{\lambda,\parallel}$	In-plane effective mass
$m^*_{\lambda,\perp}$	z-directional effective mass

m_{rel}	Relative OAM quantum number
n	ρ-directional quantum number
N_ν^S	Plasma contribution for PL
$\mathcal{O}$	General operator
$\mathbf{q}$	3-D wave vector
q	Length of wave vector
$q_\parallel$	In-plane component of $\mathbf{q}$
$q_\perp$	z directional component of $\mathbf{q}$
R	Average radius of a quantum ring
$\mathbf{r}$	Spatial position vector in 3-D space
$\mathbf{r}_\parallel$	In-plane position vector
$\mathcal{S}$	Quantization area
S	Index for singlet contribution terms
T	Index for triplet contribution terms
t	Time
$U_\lambda(\mathbf{r})$	Confinement potential
$U_\parallel^\lambda(\rho)$	ρ-directional effective confinement potential
$\mathbf{u_q}(\mathbf{r})$	Mode function of light
$\mathcal{V}$	Quantization volume
V	Functional of expectation value dynamics
v	Valence band
$V_{i_1,i_2;i_3,i_4}^{\lambda;\lambda'}$	Coulomb matrix element
$w_\lambda(\mathbf{r})$	Crystal periodic Bloch function
z	z coordinate in Cartesian/cylindrical coordinate system

1. Introduction

1.1 Background

The progress in nanofabrication techniques during the past decades has opened the possibilities to manufacture wide variety of semiconductor quantum structures with reduced dimensionality. In general, these structures can be divided into quantum-well (QW), quantum-wire (QWI) and quantum-dot (QD) structures that are quasi-two-, one- and zero-dimensional systems, respectively. The oldest and the most studied of these structures is QW, which history dates back to the 70's when the first experimental verifications of these heterostructures where made [1, 2]. The applications of various quantum structures include several different types of lasers [3–5], solar cells [6, 7], memories for data storage [8–10] and single-electron devices [11–13], to name only a few examples.

Theoretical work on the physics of semiconductor nanostructures spans over several subfields ranging from the band-structure and quantum-confinement calculations to formulation of suitable many-body theories [14, 15]. It is highly important to study and develop these theoretical approaches in order to understand the fundamentals of physical phenomena occurring in these systems. The obtained knowledge is not only usable to characterize and enhance the properties of the fabricated structures, but it can be also applied to design completely novel devices to meet emerging technological demands. This theoretical research has already opened new fields of physics, including the semiconductor quantum optics [15], and proven its importance through several applications, like the quantum cascade laser [16], that were predicted before any experimental demonstrations.

To study the fundamental properties of semiconductor optoelectronic devices, it is essential to understand the details of light–matter interactions in these systems and how the properties of electronic states change in optical transitions. In semiconductors, the optical transitions cover the energy range from millielectron volts of intraband transitions up to electron volts related to interband processes. This thesis is divided into two branches where the optical transitions that drastically change spatial properties of electrons are studied in two model systems. In the first system, interband transitions are studied in quantum-ring (QR) structures with submicrometer diameters. The second system consists of a double-QW structure with both type-I and type-II characteristics, where holes, i.e. missing valence band electrons, are confined to one of the wells whereas conduction band electrons can be in either of the QWs. In this system, the study is focused on intraband transitions.

Properties of the structures similar to those of the two model systems have been intensively studied during the last decades, as discussed in Chapters 3 and 4. However, one common feature between the studied systems is that they seem to lack systematic microscopic studies on the so called doublet level [15]. This level of quantum-mechanical theory is needed, e.g., to accurately study the properties of incoherent excitons and light fields [15]. These again are required for proper modeling of several processes related to the inter- and intraband transitions, like photoluminescence (PL) emitted from excited states [15] and transitions between exciton states [17].

1.2 Objectives and scope

The main aim of this thesis work is the formulation of microscopic theories for the model systems on the doublet-level accuracy and to use these theories to find new effects that can be utilized for optoelectronic applications. Based on the preliminary results obtained from the theoretical models, two additional primary objectives for this thesis emerged. In the QR system, this objective is the demonstration of orbital-angular-momentum (OAM) coupling between the ring and the optical field, even in the case of plane-wave modes of light. The corresponding aim in the QW system was found to be the proving of the plausibility of a selective transport of different excitations through internal interfaces of heterostructures.

All the relevant research questions are treated in six journal articles. For the QR system, this thesis includes results starting from the characterization of single-particle (SP) properties of carrier states (electrons and holes) presented in Publication I. The interband transitions where a classical plane-wave field induces OAM change of electronic states is studied in Publication II. In Publication III, the quantized optical field is introduced to provide the luminescence Elliott formula [15] that can be applied to arbitrary light modes and semiconductor structures. This formula is used in Publication IV to demonstrate the detectability of light–matter OAM coupling in QRs via angle-resolved PL. Publication V concentrates on the double-QW structures, where also a novel idea of a pure correlation-transport effect is demonstrated. The topic of Publication VI considerably differs from the main themes of the thesis. However, the quantum-mechanical SP problems, considered in this work, and the electrodynamics of the ring-resonator system studied in Publication VI have many similarities, which naturally connects these works. Throughout this work, the practical applicability of the results are considered by choosing realizable or existing structures whenever numerical results are computed.

The research methods used in this work are based on the envelop-function formalism [14] used to find the SP properties of electrons and holes. The related many-body problems are studied in the second quantization, where the emerging hierarchy problem is handled with the cluster-expansion approach [15]. The used methods are summarized in Chapter 2, which also includes a brief summary of the connection between SP quantum mechanics and the propagation of electromagnetic waves in photonic integrated circuits. The main results of the thesis are represented in Chapters 3 and 4 for the QR and QW systems, respectively. The thesis is concluded in Chapter 5 with the discussion of possible application schemes for the found effects and directions for further research.

2. Theoretical concepts

The optical and electronic properties of semiconductors involves always a quantum-mechanical many-body problem. It is usually beneficial to model these properties by introducing quasiparticle states that include many-body interactions while they otherwise resemble elementary particles. For example, the excitons, which are important for optical properties, are quasiparticle states formed by Coulomb-interacting electrons and holes [18]. Even the charge carriers, which are here considered as SP states, are not elementary particles but rather quasiparticles that include features like the electron–ion Coulomb interactions [15].

The second quantization is the most common method to formulate many-body theories in semiconductor systems. The benefits of using this method include the systematic way to handle creation and annihilation of charge carriers and quasiparticles, resulting from the coupling with electromagnetic fields. The formulation of second-quantization models involves matrix elements that are related to the solutions of the SP states. Thus, the many-body problems in semiconductors can be approached by first solving the properties of electronic states. Furthermore, the dynamics of a many-body system always introduces the Bogoliubov-Born-Green-Kirkwood-Yvon (BBGKY) hierarchy problem, which in general cannot be explicitly solved [15]. In this thesis, the cluster-expansion approach [17] is used to resolve the BBGKY problem and to provide approximate solutions for many-body dynamics.

In this Chapter, the theoretical methods used in this thesis to solve the described issues are summarized. The presentation is started from the envelope-function approximation for the SP states in quantum structures. This is followed by the description of the used optical fields and the second-quantization system Hamiltonians. At the end, a short description of the cluster-expansion approach is given.

2.1 Carrier states in nanostructures

In this work, the envelope-function approach is used to model the single-particle properties. This approach for quantum structures was introduced by Bastard [19, 20] and more explicitly studied by Burt [21–23] and several other authors [24–26]. The simplest form of the envelope-function approximation is adopted in this thesis by assuming that the wave functions $\psi_{\lambda,i}(\mathbf{r})$ for electronic states are given by

$$\psi_{\lambda,i}(\mathbf{r}) = \xi_{\lambda,i}(\mathbf{r}) w_\lambda(\mathbf{r}), \tag{2.1}$$

where $\xi_{\lambda,i}(\mathbf{r})$ is the envelope-function part defined by the quantum number (λ, i) and $w_\lambda(\mathbf{r})$ is the crystal periodic Bloch function at the Γ-point of the Brillouin zone [14]. In addition, the two-band approximation is used where the band index λ can only have values $\lambda = c$ or $\lambda = v$ for the energetically lowest conduction and highest valence band, respectively. Also the band index $\lambda = h$ is used for the holes that correspond to missing electrons in the band $\lambda = v$. The used approximation is valid when the properties involving the conduction and valence band electrons close enough the band edges are studied and all the other bands are energetically well separated from the bands $\lambda = c$ and $\lambda = v$ at the Γ-point.

The index i, appearing in Eq. (2.1), is a set of three quantum numbers in the most general case where all spatial dimensions are considered. If the movement of carriers is restricted in one or more dimensions, the corresponding parts of the envelope functions are called as confinement functions. For example, in QWs where carriers are confined in z direction, the envelope function is given by $\xi_{\lambda,i}(\mathbf{r}) = \mathrm{e}^{\mathrm{i}\mathbf{k}_\parallel \cdot \mathbf{r}_\parallel} \xi_{\lambda,l}(z)/\sqrt{\mathcal{S}}$, where $\xi_{\lambda,l}(z)$ is the confinement function defined by the confinement index l that can have only discrete values for truly confined states. In here, $\mathcal{S}$ is the quantization area and the remnant part of the index i is given by the two-dimensional quantum number $\mathbf{k}_\parallel$ that defines the momentum of the electronic state in the QW plane, in which $\mathbf{r}_\parallel$ defines the spatial location.

The envelope functions are solved from the effective-mass Shrödinger equation

$$\left[-\frac{\hbar^2}{2m^*_{\lambda,\parallel}} \nabla^2_\parallel - \frac{\hbar^2}{2m^*_{\lambda,\perp}} \frac{\partial^2}{\partial z^2} + U_\lambda(\mathbf{r}) \right] \xi_{\lambda,i}(\mathbf{r}) = E_{\lambda,i} \xi_{\lambda,i}(\mathbf{r}), \tag{2.2}$$

where $E_{\lambda,i}$ is the SP energy, $U_\lambda(\mathbf{r})$ is the confinement potential and $m^*_{\lambda,\parallel}$ is the effective mass of the band λ in the structure plane that is always selected to be perpendicular to the z axis. The corresponding mass to

the growth direction is denoted by $m^*_{\lambda,\perp}$ and $\nabla^2_{\parallel}$ is the two-dimensional Laplace operator in the x-y plane. When formulating Eq. (2.2), similar steps are taken as in Ref. [22] for the band that is energetically well separated from all other bands. Furthermore, the interface contributions and the spatial and energetic dependence of the effective mass is omitted. In addition, $U_\lambda(\mathbf{r})$ is assumed to be given directly by the band offsets between the materials used for the structures. These are rather well justified approximations when considering SP states that are strongly confined inside the structures and that are energetically near the band edges.

When numerical values for the effective masses and confinement potentials are needed, the following approach is used. The same eight bands as in the Kane's $\mathbf{k}\cdot\mathbf{p}$ method [27] are selected for a more detailed study, whereas the effects of the other bands are included only through the Löwdin's perturbation theory [28]. As the studied structures are always thinner than the critical thickness, the materials of the structures can be assumed to be strained [29, 30]. The effects of strain are studied by following the steps in Ref. [31] where the approach of Pikus and Bir [32] is applied for zincblende materials. At this stage, also some additional approximations are included, like the omission of terms causing non-parabolicity of the bands. As a result, the strain correlated band energies are found for the $U_\lambda(\mathbf{r})$ and for the effective masses. In addition, the approach yields the heavy-hole–light-hole energy splitting at the Γ point, which can also be caused solely by the confinement effects. This splitting inflicts the mass-reversal effect where the highest energy hole band has $m^*_{h,\perp}$ close to the bulk heavy-hole mass while $m^*_{h,\parallel}$ can approach the mass of bulk light-hole band [30, 33–35].

The most beneficial reasons of using the above described method to obtain approximate effective-mass values is based on numerical simplicity simultaneously as it can be assumed to give more accurate results than by just using the corresponding bulk values, e.g. it gives the mass reversal that has also been experimentally detected. Furthermore, in the absence of experimentally measured band parameters for the systems studied in here, all the needed parameters for the described approach are quite well documented for the considered III-V compounds. In this work, the parameters from Refs. [36, 37] are used. Since the focus of the thesis is in the finding of qualitatively new effects that mostly depend on the geometry of $U_\lambda(\mathbf{r})$, a more detailed SP studies were omitted.

2.2 Connection between the quantum mechanics of electronic states and the propagation of waves in photonics

The way light propagates in integrated photonic circuits is determined by the four classical Maxwell equations. By making three following assumptions regarding the studied system, one is able to see the connection between the wave equation for light modes and the Schrödinger equation studied in the previous section. The first assumption is related to the field intensities that are assumed to be small enough, so that the nonlinear optics is not needed. Secondly, the material should be macroscopic and isotropic in a sense that one can relate the electric and the displacement fields by multiplying with a real valued scalar dielectric function $\varepsilon(\mathbf{r})$, where explicit dependence on field frequency ω is omitted. Finally, only harmonic modes with time dependence given by $\mathrm{e}^{-\mathrm{i}\omega t}$ are considered. With these assumptions, Maxwell's equations lead to the wave equation for modes of the magnetic field, $\mathbf{H}(\mathbf{r})$, that is given by [38]

$$\nabla \times \left(\frac{1}{\varepsilon(\mathbf{r})} \nabla \times \mathbf{H}(\mathbf{r}) \right) = \left(\frac{\omega}{c_0} \right)^2 \mathbf{H}(\mathbf{r}), \tag{2.3}$$

where c_0 is the vacuum speed of light.

If one compares the above equation to Eq. (2.2), it is found that Eq. (2.3) is a generalization of the effective mass Scrödinger equation. Both equations are eigenvalue problems, even though the one is for scalar and the other one for vector eigenfunctions. In Eq. (2.2), the SP carrier energies, $E_{\lambda,i}$, are the eigenvalues of the problem while in the equation for $\mathbf{H}(\mathbf{r})$ the corresponding values are the frequencies ω of the harmonic modes. In addition, carrier states of semiconductor structures are confined to locations where $U_\lambda(\mathbf{r})$ has a minimum. A similar effect in Eq. (2.3) is caused by $\varepsilon(\mathbf{r})$, where the light modes are concentrated into regions with high values of a dielectric constant. A more comprehensive comparison between these two system, especially in case of spatially periodic potentials and dielectric constants, is given in Ref. [38].

In this thesis, qualitative solutions of Eq. (2.3) were analytically studied for the ring-resonator system in Publication VI. To some extent, this study resembled the work done in Publication I. The obtained results were used to improve the performance of fully numerical modeling of the system, which included Eq. (2.3) explicitly. Furthermore, analytical approaches based on solutions of Eq. (2.3) were used to study the nature of the equations of transmission characteristics of ring resonators [39]. These equations were then used in Publication VI to interpret experimen-

tal results and to reduce the time needed to find near-optimal structures for polarization independent broad-bandwidth ring-resonator systems.

2.3 Treatment of optical field

In this thesis, the $\mathbf{E}\cdot\mathbf{r}$ picture [15] is used to describe the light–matter interactions by using either classical or quantized electric field $\mathbf{E}(\mathbf{r},t)$. The simplest form of the field, used in Publication V, is the classical terahertz (THz) field given by $\mathbf{E}(t) = E_0\cos(\omega t)\hat{\mathbf{e}}_z$, where the spatial dependency of the field is omitted, E_0 is the amplitude of the field and $\hat{\mathbf{e}}_z$ is the unit vector to the z direction. A more general classical field is studied in Publication II, where the field is given by its Fourier series expansion: $\mathbf{E}(\mathbf{r},t) = \sum_{\mathbf{q}} E_{\mathbf{q}}(t)\mathrm{e}^{\mathrm{i}\mathbf{q}\cdot\mathbf{r}}\hat{\mathbf{e}}_{\parallel}$. In this equation, $\mathbf{q}$ is the wave vector of the plane-wave component of the field, $\hat{\mathbf{e}}_{\parallel}$ is the polarization vector of the field that is always assumed to be in the plane of the structure and the time dependence is included in the amplitude term $E_{\mathbf{q}}(t)$. Throughout this work, the wavelengths connected to the $\mathbf{q}$ modes are assumed to be reduced from their vacuum values by the refractive index of the system.

A quantum description of light is needed when PL emitted from a semiconductor quantum structure is studied [15]. In the second quantization, the optical field can be given by [15]

$$\mathbf{E}(\mathbf{r},t) = \mathrm{i}\sum_{\mathbf{q}} \mathrm{E}_{\mathbf{q}}\left[\mathbf{u}_{\mathbf{q}}(\mathbf{r})B_{\mathbf{q}} - \mathbf{u}^{*}_{\mathbf{q}}(\mathbf{r})B^{\dagger}_{\mathbf{q}}\right], \tag{2.4}$$

where $\mathrm{E}_{\mathbf{q}}$ is the vacuum field amplitude and $\mathbf{u}_{\mathbf{q}}(\mathbf{r})$ is the mode function. The time dependence of the quantized field is within the dynamics of photon annihilation, $B_{\mathbf{q}}$, and creation, $B^{\dagger}_{\mathbf{q}}$, operators.

Even though any possible mode basis in Coulomb gauge was considered for Publication III, all numerical results in Publications III-V are obtained in the plane-wave basis. In this basis, the mode functions are given by $\mathbf{u}_{\mathbf{q}}(\mathbf{r}) = \mathrm{e}^{\mathrm{i}\mathbf{q}\cdot\mathbf{r}}\hat{\mathbf{e}}_{\mathbf{q}}/\sqrt{\mathcal{V}}$, where $\mathcal{V}$ is the quantization volume and $\hat{\mathbf{e}}_{\mathbf{q}}$ is the polarization vector of the mode. Furthermore, for all QR results, the polarization of modes were again selected to fulfill $\hat{\mathbf{e}}_{\mathbf{q}} = \hat{\mathbf{e}}_{\parallel}$.

2.4 System Hamiltonians

The modeling of many-body effects in studied structures is started from the second-quantization system Hamiltonian H that is given by the equation [15]

$$H = H_0 + H_{\mathrm{C}} + H_{\mathrm{D}}. \tag{2.5}$$

This Hamiltonian includes the contribution from the non-interacting carriers and photons

$$H_0 = \sum_{\lambda,i} E_{\lambda,i} a^{\dagger}_{\lambda,i} a_{\lambda,i} + \sum_{\mathbf{q}} \hbar\omega_{\mathbf{q}} \left(B^{\dagger}_{\mathbf{q}} B_{\mathbf{q}} + \frac{1}{2} \right), \tag{2.6}$$

where $a^{\dagger}_{\lambda,i}$ and $a_{\lambda,i}$ are the creation and annihilation operators, respectively, for the carrier identified by index (λ, i). For the classical fields, the contribution $\sum_{\mathbf{q}} \hbar\omega_{\mathbf{q}}(B^{\dagger}_{\mathbf{q}} B_{\mathbf{q}} + 1/2)$ is naturally omitted. The interactions between the carriers are included in

$$H_{\mathrm{C}} = \frac{1}{2} \sum_{\lambda,\lambda'} \sum_{i_1,i_2,i_3,i_4} V^{\lambda;\lambda'}_{i_1,i_2;i_3,i_4} a^{\dagger}_{\lambda,i_1} a^{\dagger}_{\lambda',i_2} a_{\lambda',i_3} a_{\lambda,i_4}, \tag{2.7}$$

which in turn includes the Coulomb matrix element (CME)

$$V^{\lambda;\lambda'}_{i_1,i_2;i_3,i_4} = \frac{e_0^2}{4\pi\varepsilon} \int \mathrm{d}^3 r \mathrm{d}^3 r' \frac{\xi^*_{\lambda,i_1}(\mathbf{r}) \xi^*_{\lambda',i_2}(\mathbf{r}') \xi_{\lambda',i_3}(\mathbf{r}') \xi_{\lambda,i_4}(\mathbf{r})}{|\mathbf{r} - \mathbf{r}'|}, \tag{2.8}$$

where e_0 is the elementary charge and ε is the dielectric constant of the system. The light–matter interaction is given by H_{D} that includes at least one of the terms $H_{\mathrm{D,class}}$, $H_{\mathrm{D,quant}}$ and $H_{\mathrm{D,THz}}$. Terms $H_{\mathrm{D,class}}$ and $H_{\mathrm{D,quant}}$ describe the optical field induced interband transitions for the classical and quantum fields, respectively. The intraband transitions driven by classical THz field are included by $H_{\mathrm{D,THz}}$. By using the optical fields of the previous section, the different dipole Hamiltonians are given by

$$H_{\mathrm{D,class}} = -\sum_{\mathbf{q},i,i'} E_{\mathbf{q}}(t) \left[d_{v,c} D^{\mathbf{q}}_{i,i'} a^{\dagger}_{v,i} a_{c,i'} + (d_{v,c} D^{-\mathbf{q}}_{i,i'})^* a^{\dagger}_{c,i'} a_{v,i} \right], \tag{2.9}$$

$$H_{\mathrm{D,quant}} = -\sum_{\mathbf{q},i,i'} \mathrm{i} \frac{\mathrm{E}_{\mathbf{q}}}{\sqrt{\mathcal{V}}} d_{v,c} \left[D^{\mathbf{q}}_{i,i'} B_{\mathbf{q}} + D^{-\mathbf{q}}_{i,i'} B^{\dagger}_{\mathbf{q}} \right] a^{\dagger}_{v,i} a_{c,i'} + \mathrm{H.c.}, \tag{2.10}$$

$$H_{\mathrm{D,THz}} = E_{\mathrm{THz}}(t) \sum_{\lambda,i,i'} \mathcal{D}^{\lambda}_{i,i'} a^{\dagger}_{\lambda,i} a_{\lambda,i'}, \tag{2.11}$$

where $d_{v,c}$ is the dipole-matrix element with respect to the crystal periodic Bloch functions [14]. In here, the vector form of $d_{v,c}$ is assumed to be parallel to the polarization vectors $\hat{\mathbf{e}}_{\mathbf{q}}$, for simplicity, and H.c. denotes the Hermitian conjugate of the term preceding it.

The dipole matrix elements (DMEs) appearing in above equations are calculated by using the method of length scale separation between the

envelope/confinement functions and the crystal periodic function [14]; the same method is also used to obtain Eq. (2.8). As a result, the highly important matrix elements for this work are given by

$$D^{\mathbf{q}}_{i,i'} = \int \mathrm{d}^3 r \xi^*_{v,i}(\mathbf{r}) \mathrm{e}^{\mathrm{i}\mathbf{q}\cdot\mathbf{r}} \xi_{c,i'}(\mathbf{r}), \tag{2.12}$$

$$\mathcal{D}^{\lambda}_{i,i'} = |e_0| \int \mathrm{d}^3 r \, \xi^*_{\lambda,i}(\mathbf{r}) z \xi_{\lambda,i'}(\mathbf{r}). \tag{2.13}$$

The described system Hamiltonian is a rather general one. The only typically used extensions for this Hamiltonian would be the inclusion of the effects given by lattice vibrations [15]. These vibrations could be described by the quantized phonon field, which would lead to similar contributions as with photons [15]. This, in turn, would lead to additional complications when numerical calculations are done. However, at low enough temperatures it can be assumed that the effects of lattice vibrations compared to the whole system are small [15] and thus they are omitted since temperatures below a few tens of Kelvins are typically considered.

2.5 Low-density Wannier equation for excitons

After solving the single particle energies and envelope/confinement functions from Eq. (2.2), and Coulomb matrix elements in Eq. (2.8), one can formulate the low-density approximation for the Wannier equation [17], which gives the excitonic states of the studied system when charge carrier densities approach zero. In the general case, this equation is given by the matrix eigenvalue problem

$$(E_{c,i'} + E_{h,i})\phi^{i,i'}_{\nu} - \sum_{i_1,i_2} V^{c;v}_{i',i_1;i,i_2} \phi^{i_1,i_2}_{\nu} = \mathcal{E}_{\nu} \phi^{i,i'}_{\nu}, \tag{2.14}$$

where $\phi^{i,i'}_{\nu}$ is the excitonic wave function for a state with energy $\mathcal{E}_{\nu}$ that is defined by the exciton index ν. The excitonic energies are given with respect to the system band gap E_g.

In the case of QW or QWI, where the movement of carriers is not restricted at least in one dimension, the center-of-mass and the relative movement of electrons and holes combined to the exciton state can be separated [15]. Consequently, the relative-movement equation is found to have one-to-one correspondence to the hydrogen problem [15], which solutions can be divided into two groups. The solutions for the relative movement that corresponds to energies below E_g are the so called bound states that are often labeled as the hydrogen states for $1s$, $2s$, $2p$, etc.

This grouping is based on symmetries of the wave functions similarly as in the atomic problem. The excitonic states where the energy of relative movement is positive are the ionized solutions of the Wannier equation. These ionized states constitute a continuous spectrum for excitonic energies in QW and QWI systems, in contrast to the bound solutions that have discrete energies.

2.6 Dynamics of observables

In quantum mechanics, the experimentally measurable results for observables can be predicted by calculating expectation values of the related operators. In semiconductor quantum optics, all observables can be connected to N-particle operators [15], which expectation values are denoted by $\langle N \rangle$. The one-particle operator corresponds either to one boson operator or to a pair of a carrier annihilation and creation operator. Thus, all one-particle expectation values, $\langle 1 \rangle$, in this thesis are given by $\langle a^\dagger_{\lambda,i} a_{\lambda',i'} \rangle$, $\langle B_\mathbf{q} \rangle$ and $\langle B^\dagger_\mathbf{q} \rangle$, whereas the N-particle expectation values for pure carrier operators have always the form $\langle a^\dagger_{\lambda_1,i_1} \cdots a^\dagger_{\lambda_N,i_N} a_{\lambda'_N,i'_N} \cdots a_{\lambda'_1,i'_1} \rangle$.

One possible approach to solve the expectation value for a general operator $\mathcal{O}$ is obtained via the Heisenberg equation of motion

$$\mathrm{i}\hbar \frac{\partial}{\partial t} \langle \mathcal{O} \rangle = \langle [\mathcal{O}, H]_- \rangle. \tag{2.15}$$

However, resulting from the structure of the system Hamiltonian defined in Eqs. (2.5)–(2.13), it follows that the dynamics of each expectation value of N-particle operator is coupled to the dynamics of $(N+1)$-particle operator expectation value. Schematically this can be expressed by

$$\mathrm{i}\hbar \frac{\partial}{\partial t} \langle N \rangle = E[\langle N \rangle] + V[\langle N \rangle + 1], \tag{2.16}$$

where the functional E mostly follows from the non-interacting parts of the system Hamiltonian while V is given by the interactions. As an example, the dynamics of one-particle electron occupation $f^e_i \equiv \langle a^\dagger_{c,i} a_{c,i} \rangle$ with respect to the Coulomb Hamiltonian is

$$\mathrm{i}\hbar \frac{\partial}{\partial t} f^e_i \Big|_{H_C} = \sum_{\lambda,i_1,i_2,i_3} V^{c;\lambda}_{i,i_1;i_2,i_3} \left(\langle a^\dagger_{c,i} a^\dagger_{\lambda,i_1} a_{\lambda,i_2} a_{c,i_3} \rangle - \langle a^\dagger_{c,i_3} a^\dagger_{\lambda,i_2} a_{\lambda,i_1} a_{c,i} \rangle \right), \tag{2.17}$$

which shows the coupling of f^e_i to the carrier two-particle operators. This coupling of dynamical equations leads to the BBGKY hierarchy problem, which introduces a continuously complicating chain of equations that cannot be closed [15, 17].

2.7 Cluster-expansion method

Assuming that all SP states as well as relevant interaction matrix elements can be solved, the hierarchy problem indicated above is basically behind all the complications in the semiconductor many-body studies, especially in systems with more than just a few possible states. As the exact solution is generally infeasible, different approximate approaches have been developed. These approaches include different methods based on the Green's functions approach, Feynman path integrals and density functional theory, to name a few examples [15]. All of these approaches have their own advantages and limitations. One of the most successful approaches in practice, especially with problems involving semiconductor quantum optics, has been the cluster-expansion method [17]. This method has been used in Publication II-V, even though in Publication II it has been adopted in the lowest level that corresponds to a more conventional Hartree-Fock approximation [14, 15].

In the cluster-expansion method, the many-body quantities are systematically grouped into so called clusters, starting from the singlets corresponding to the one-particle expectation values $\langle 1\rangle$. The second level in cluster expansion is the inclusion of doublets that consist of expectation values of creation/annihilation operators of interacting pairs of particles. This grouping of different clusters with increasing complexity can be continued to the desired level, which includes the expectation values of a generic N-particle operator. The described recursive scheme can be expressed by [17]

$$\begin{aligned}
\langle 1\rangle =&[\langle 1\rangle]_S \\
\langle 2\rangle =&[\langle 2\rangle]_S + \Delta\langle 2\rangle \\
\langle 3\rangle =&[\langle 3\rangle]_S + \langle 1\rangle\Delta\langle 2\rangle + \Delta\langle 3\rangle \\
\langle N\rangle =&[\langle N\rangle]_S + [\langle N-2\rangle_S\Delta\langle 2\rangle + \langle N-4\rangle_S\Delta\langle 2\rangle\Delta\langle 2\rangle + \cdots]_D \\
&+ [\langle N-3\rangle_S\Delta\langle 3\rangle + \langle N-5\rangle_S\Delta\langle 3\rangle\Delta\langle 2\rangle + \cdots]_T \\
&+ \sum_{J=4}^{N-1}[\langle N\rangle]_J + \Delta\langle N\rangle,
\end{aligned} \tag{2.18}$$

where the subscripts S, D, T and J denote singlet, doublet, triplet and higher-order contributions, respectively. The introduced $\Delta\langle N\rangle$ terms include the purely correlated parts of the N-particle expectation values and it is obtained by subtracting all lower-order terms from the total expectation value $\langle N\rangle$. In the above equations, the singlet part $\langle N\rangle_S$ for carrier

operators involves the Hartree-Fock factorization; also the cluster products contain all combinations of factorization [17].

The overall success of the cluster-expansion method relays on the fact that for many theoretically and experimentally approachable systems one can restrict the analysis to a certain cluster level. For example, if the optical properties of the system can be assumed to be characterized by SP carriers and excitons, one can restrict considerations to the doublet level that includes the dynamics of desired quasiparticle states explicitly while the next generation of clusters can be phenomenologically described. This truncation of the scheme in Eq. (2.18) provides a closed set of dynamical equations that can be solved at least numerically.

Similarly as with the other approaches to solve the hierarchy problem, the explicit cluster-expansion faces difficulties in larger systems, especially when one moves beyond the singlet level. In more detail, the full singlet-doublet factorization itself includes a vast number of closed equations [17], which generally make the system unfeasible for numerical solution. However, since one can address different types of cluster contributions to be describe particular kinds of processes, their contribution to the total system can often be analyzed without solving them explicitly. This gives an opportunity to introduce additional approximations, like the homogeneity of carrier excitation distribution and the main-sum approximation [15, 17], which significantly reduce the complexity of the problem leading to a solvable system.

3. Quantum rings and the change of carrier rotational characters

Resulting from the work of Aharonov and Bohm [40], quantum systems with toroidal topology have gained a lot of interest. In these systems, the phase of the wave function of electron is dependent on the magnetic flux penetrating the structure, even when the magnetic field itself does not overlap with the electronic wave functions [40]. In addition to Aharonov-Bohm effect, it is possible to detect the related persistent currents [41–43] in ring like systems.

In late 90's, a new electronic system with toroidal topology was introduced when the first semiconductor quantum rings where fabricated [44]. These rings were made unintentionally during a QD growth, utilizing the Stranski-Krastanov self-assembly process. Since then, there has been several different demonstrations of the suitability of different self-assembly [45–48] and even lithographic [49, 50] methods to fabricate QRs from various semiconductor materials with different geometries.

The possibilities of using micro- and nanofabrication processes to produce ring systems with desired properties has been one of the main reasons for the studies on QRs. Similarly as with the semiconductor QDs, this enables one to study systems with properties similar to the elementary atoms or molecules, which characters cannot be specifically adjusted. With quantum rings, tailoring of physical properties led to a considerable interest in theoretical and experimental studies of demonstrating Aharonov-Bohm-like effects. This inspiration has continued until recent years [49–56].

In addition to the studies directly involving effects observable in magnetic fields, there has been also numerous studies based on the solutions of SP states of QRs [57–61]. Furthermore, optical properties [62–65] including PL [46, 49, 54, 66–69] of QRs have been subject of interest together with effects found under the influence of static electric fields

[58, 70, 71]. One of the most recent field of study involving the ring structures has been their coupling to the angular momentum properties of light, especially to the OAM of light [72, 73].

In this chapter, based on the results in Publications I-IV, several properties of QRs are represented. The single-particle and excitonic states in QRs are reviewed. The distinction between the coupling of the OAM of light between QRs and QDs are discussed, with a short summary about OAM properties of light. In the end, angle-resolved absorption and emission of QR are demonstrated, which are connected to the change of rotational properties of electrons and to the coupling between QRs and OAM of light.

3.1 Single-particle states in QRs

One possible definition for a semiconductor quantum ring can be given by three characteristics. First, the system should be circularly symmetric. From this it follows that the carrier states in QR are eigenstates of OAM with respect to the symmetry axis of the ring. The second feature is that the volume of QR should be small enough to provide a fully quantized energy spectrum for the carriers, in contrast to typical QWs and QWIs. Finally, the ring structure should have the toroidal topology.

The symmetry requirement is never exactly fulfilled in real structures that always show some asymmetry [44, 51, 53]. Hence, it is more important that the fabricated structures are symmetric enough so that the qualitative results follows the predictions given by the simplified model. The effects of asymmetries in contrast to the idealized structure have been widely studied and it has been shown that the structures can have considerable imperfections and still follow the properties of fully symmetric rings [53, 55, 58, 74–77].

As the second characteristic of QR is the definition of a quasi-zero-dimensional structure, QRs can be seen as a subcategory of QDs. The distinction between a common QD and a ring follows from the third criteria. The central hole makes it possible to fabricate QRs with submicrometer diameters that still show clearly quantized SP spectra. By contrast, the fully quantized nature of dot systems can be assumed to be drastically reduced by the increasing volume in QDs with similar diameters. From the same distinguishing topological feature, it follows that the interaction between the optical fields and QRs or QDs can be qualitatively quite

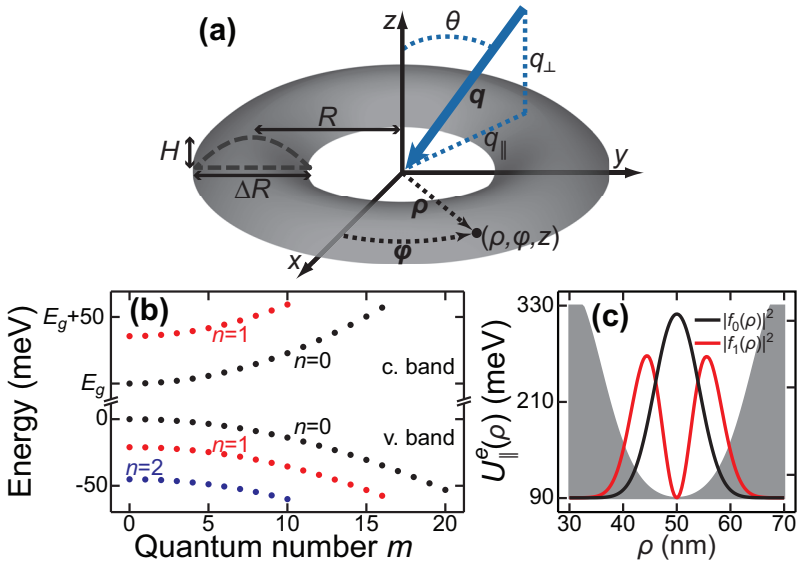

Figure 3.1. Quantum ring structure and single-particle properties. (a) The QR geometry is characterized by the radius R, lateral thickness ΔR and height H. The system is studied in cylindrical coordinate system (ρ, φ, z) where the z and QR symmetry axes are the same. Propagation direction of the studied light modes are defined by the wave vector $\mathbf{q}$ that forms the angle θ with the symmetry axis. The QR-plane and z-directional components of the wave vector are denoted by $q_{\parallel}$ and $q_{\perp}$, respectively. (b) The single-particle energy spectrum shows approximate quadratic dependence on OAM quantum number m and linear dependence on quantum number n that defines the radial excitations. (c) The effective radial confinement potential for electrons (shaded area) is almost harmonic. This results in that the effective radial confinement functions for the ground state (black line) and first excited n subband (red line) equal to the corresponding wave functions of the harmonic oscillator.

different, as discussed later.

To study the properties of SP states in QRs more explicitly, it is beneficial to use the symmetry of the ring and solve the Schrödinger equation (2.2) in cylindrical coordinates (ρ, φ, z), where the z axis is selected to equal the symmetry axis of the ring, as depicted in Fig. 3.1(a). In this figure, also other coordinates are defined together with the geometrical parameters of the ring. These parameters are the average radius R, the lateral thickness ΔR and the height H of the QR structure. Furthermore, Fig. 3.1(a) illustrates the wave vector $\mathbf{q}$ that forms an angle θ with the symmetry axis of the ring. This vector that defines the propagation direction of light modes is needed in the following sections with its components $q_{\parallel}$ and $q_{\perp}$.

By utilizing the assumed symmetry of QRs, one can separate the φ dependence in Eq. (2.2) to give a three-dimensional confinement function

$\xi_{\lambda,i}(\mathbf{r}) = \mathrm{e}^{\mathrm{i}m\varphi}\xi_{\lambda,n,m}(\rho,z)/\sqrt{2\pi}$, where the index i is now divided into two indexes n and m. In here, the highly important OAM quantum number m emerges, which can have only integer values. It describes how the carrier states are rotating around the symmetry axis. In addition, the separation of φ dependence gives an approximate energy contribution $\hbar^2m^2/(2m^*_{\lambda,\|}R^2)$ for the single particle states that would be the exact SP energy if an infinitely thin QR were assumed [78]. This quadratic energy dependence can be seen in Fig. 3.1(b), where the energy spectrum for a ring with $R = 50$ nm, $\Delta R = 35$ nm and $H = 3$ nm is shown. This particular ring configuration has been used for all presented numerical results in this chapter. The more detailed geometry and material properties of the GaAs model ring can be found from Publication IV, where similar QR has been considered.

Semiconductor quantum rings are generally flat structures, $H \ll \Delta R$, with the height of only a few nanometers. This property can be used for two results. As only the carrier states near the edges of v and c bands are considered, one can assume that the system remains always in the ground state with respect to the z direction and relate the quantum number n to the ρ-directional excitations only. Another result following from the flat ρ-z cross-section is an approximate separability of the confinements with respect to these coordinates, i.e. one can formulate an approximate solution $\xi_{\lambda,n,m}(\rho,z) = f_{\lambda,n,m}(\rho)g_{\lambda,n,m}(z)/\sqrt{\rho}$. This separability assumption was found to hold for all studied systems in this work. The applicability of the ansatz is studied in more detail in Publication I, where it is also shown how one can obtain accurate approximations for functions $f_{\lambda,n,m}(\rho)$ and $g_{\lambda,n,m}(z)$ by fully analytical methods by using only the geometry and material parameters of the system.

In Publication I, it is shown how the $\sqrt{\rho}$-factor in the ansatz for the function $\xi_{\lambda,n,m}(\rho,z)$ leads to a system where the ρ-z plane problem in cylindrical coordinates is effectively changed to a problem in common two-dimensional Cartesian coordinate system. Furthermore, in this article it is verified that the functions $f_{\lambda,n,m}(\rho)$ and $g_{\lambda,n,m}(z)$ can be approximated with the solutions of a harmonic-oscillator problem, and how these functions are defined by effective confinement potentials. Especially, the effective ρ-directional potential for the SP ground state, $U^{\lambda}_{\|}(\rho)$, is typically found to be very close to the potential of a harmonic oscillator, as shown by the shaded area in Fig. 3.1(c). This figure also depicts the squares of effective ρ-directional confinement functions, $f_n(\rho) \equiv f_{c,n,0}(\rho)$, for $n = 0$ and

$n = 1$ electrons by the black and red lines, respectively, showing the similarity to wave functions of the corresponding oscillator. This similarity of the problems can also be seen in Fig. 3.1(b), where the SP energies are almost linearly dependent on the quantum number n. This type of energy dependence has already been found by several other authors [46, 62], but the results in Publication I can be used to derive the geometry and material dependent correlations to this n dependence of the SP spectrum, as well as to the approximately quadratic m dependence.

Fully analytical solutions for the two- and three-dimensional QRs have been studied explicitly in geometries where Eq. (2.2) is fully separable; see e.g. Refs. [58, 61]. However, the approximate scheme presented in here has some benefits over these explicit solutions. The approximate solutions can be obtained fully analytically with an accuracy suitable for further studies on optical properties of QRs with frequencies in the spectral vicinity of the system band gap. This was verified for several hundreds of numerically solved QRs with parabolic cross-section, covering almost all possible III-V material configurations with reasonable values of R, ΔR and H. In contrast, the more explicit approaches typically involve transcendental equations that require numerical solutions. In addition, the found harmonic-oscillator solutions are more suitable for further calculations, which are needed for the interaction matrix elements, compared to the more complicated exact solutions. This is partly based on the fact that the harmonic oscillator is perhaps the most studied quantum system. Thus, there are a vast number of results that can be applied to QRs after the approximation for SP states are made. For an example, there are several analytical methods to approach integrals involving wave functions of harmonic oscillators [79, 80].

3.2 Coulomb interactions and excitonic states in quantum rings

The explicit equation for the Coulomb matrix element in Eq. (2.8) for QRs cannot be reduced further than a five dimensional integral. Even though the numerical solution for a single CME is a straightforward problem, the number of needed integrals in a QR system grows to the fourth power of included single-particle states. As a result, the explicit computation of all CMEs in a large size QR becomes a challenging numerical problem. With the help of the analytical confinement functions, given in previous section, the dimensionality of CME integrals can be reduced by one, which

typically leads to the reduction of the computational time by two orders of magnitude. However, this possibility has not been utilized in this thesis, but rather the analytical confinement functions have been used to study the validity of an approximate selection rule of CMEs, which leads to much greater saving in time used for numerical calculations. In detail, the selection rule is the omission of electron and hole n subband changing CMEs. Similar selection rule holds also for QWs and QWIs [17].

In addition to the described approximate selection rule, there is also a highly important explicit rule, which says that the Coulomb interaction does not change the total OAM of the interacting particles. From this selection rule, it follows that when the excitonic states are solved from the Wannier equation (2.14), the excitonic solutions are eigenstates of OAM. Thus, the resulting wave functions with components $\phi_{M,\nu}^{l_e,l_h}$ can be characterized by the exciton indexes M and ν, where $\hbar M$ is now the center-of-mass OAM of the excitonic state and ν defines the exact state inside each M channel. In here, $M = m_e + m_h$, where m_e and m_h are OAM quantum numbers for electrons and holes contributing to the excitonic state, respectively. For simplicity, it is assumed that only $n = 0$ subband is relevant in here and thus it is suppressed from explicit notations.

It was found that in QRs of a sufficiently large radii, the Wannier equation is approximately separable between the center-of-mass OAM and relative OAM, $\hbar m_{\text{rel}}$, between electrons and holes, where this relative OAM is defined by $m_{\text{rel}} \equiv (m_{h,\parallel}^* m_e - m_{e,\parallel}^* m_h)/(m_{e,\parallel}^* + m_{h,\parallel}^*)$. This is a similar separation as discussed in Section 2.5 for QWs and QWIs, where the distinction between center-of-mass and relative movement can be done explicitly. As a result, also in studied QRs the excitonic solutions can be divided into two groups: to bound excitons and to ionized solutions. Furthermore, the index ν can be used to define $1s$, $2s$, $2p$, etc. bound solutions also in QRs.

Figure 3.2(a) shows numerically solved exciton wave functions of the model QR for $M = 0$ (black dots) and $M = 3$ (red dots) $1s$ excitons as a function of m_{rel}. It can be found that these bound state solutions are highly similar. Consequently the oscillatory strengths, $\mathcal{F}_{M,\nu} \equiv \sum_{l_e,l_h} \phi_{M,\nu}^{l_e,l_h}$, for the $\nu = 1s$ states are approximately independent on M. It is also evident that the heavily Coulomb influenced $1s$ wave functions are spread over multiple electron–hole-pair combinations, in contrast to the ionized states, of which one is depicted in Fig. 3.2(a) by gray bars. This indicates that the oscillatory strength of the $1s$ states is much higher than the corresponding value of the ionized states. This can be clearly seen in the

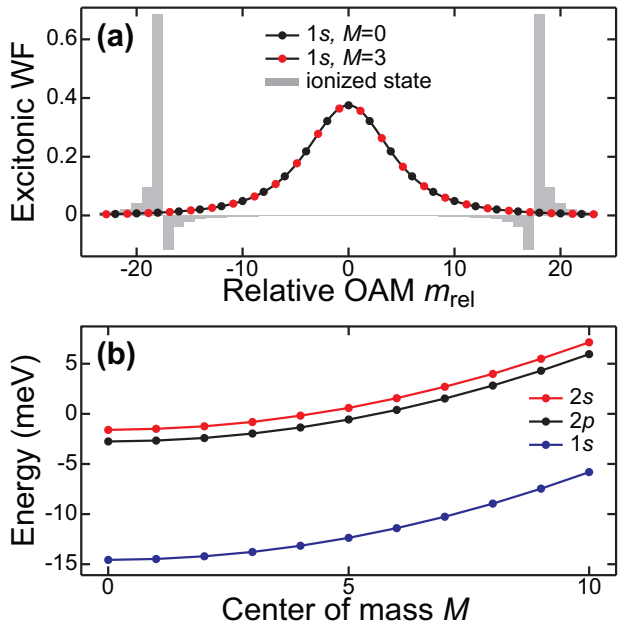

Figure 3.2. Properties of QR excitons. (a) Exciton states as a function of relative OAM m_{rel} for bound $1s$ solutions with center-of-mass OAM $M = 0$ (black dots) and $M = 3$ (red dots). For clarity, only every second m contribution is shown; the unshown points follow the black line. Gray bars show one of the ionized solutions for $M = 0$. (b) Bound exciton energies respect the band-gap are shown as a function of M for the $1s$ (blue dots), $2s$ (red dots) and $2p$ (black dots) states. Following from the fully quantized QR system, only the dots show actual results whereas the lines are for helping the illustration in both figures (a) and (b).

absorption results summarized in Section 3.4.

Another result that follows from the separability of the center-of-mass and relative OAM in studied QRs is that the energy differences between different bound state solutions are given by the center-of-mass OAM energies $\hbar^2 M^2/[2(m_{e,\parallel} + m_{h,\parallel})R^2]$. This dependence is shown in Fig. 3.2(b), where $1s$ (blue dots), $2s$ (red dots) and $2p$ (black dots) energies are illustrated with respect to the band gap of the system. As the coefficient of this OAM energy is inversely proportional to the square of the radius and as large radius QRs are studied in this thesis, it follows that the different M channels for optically bright bound excitons are hard to separate in optical spectra. A similar restriction does not hold for ionized states that can have quite large energy spacings between different M values. These energy based considerations are also discussed in more detail in the section that describes absorption results.

3.3 QRs and OAM changing transitions

To study the effects caused by optical-field-induced interband transitions in semiconductor quantum structures, it is of primary importance to calculate the dipole matrix elements in Eq. (2.12). While these results depend on the light mode under consideration, also the spatial extent of envelope/confinement functions is important. There is one type of nanostructure category where the values of Eq. (2.12) always have the same form. These are the QDs, especially the small ones, but also in larger systems the confinement functions are typically confined to the central region of the dot with a confinement function spreading much smaller than typical wavelengths of optical fields. In this case, the values of Eq. (2.12) are independent on the light modes and solely given by the overlapping integrals between electron and hole states. As a result, at this level of approximations, the plane waves cannot cause transitions where OAM is changed. Similar approach can be applied for QWs and QWIs with respect to their confinement functions, and also for QRs that have a diameter that is considerably smaller than the wavelength of the optical field.

In this thesis, the focus is in QRs with diameters larger than 70 nm. Simultaneously, the effective wavelengths of interest, reduced from their vacuum value by the background refractive index, can be as short as 150 nm. In this case, one cannot apply the similar approach as with QDs, especially when the modes are not propagating parallel to the QR symmetry axis; i.e. when the angle θ, defined in Fig. 3.1(a), is not equal to zero. Thus, each DME in Eq. (2.12) has to be carefully calculated for sufficiently large QRs. The results following from going beyond the QD dipole approximation for QR is behind the main results in Publications II-IV.

In Publication II, it was found that the explicit computation of DMEs in quantum-ring systems results in notable effects that need interband transitions where the OAM of electronic states is changed even in the case of a plane-wave field. It is a well known fact that a circularly polarized plane-wave field carries intrinsic spin angular momentum of $\pm\hbar$ with respect to the propagation direction, and that a plane-wave field in average does not carry any additional angular momentum [81]. Thus, linearly polarized light which is a superposition of the circulating modes, can produce transitions between heavy holes and electrons, where the angular momentum is changed by the quantity $\pm\hbar$. But where does the additional angular momentum emerge needed for the interband transitions that change the

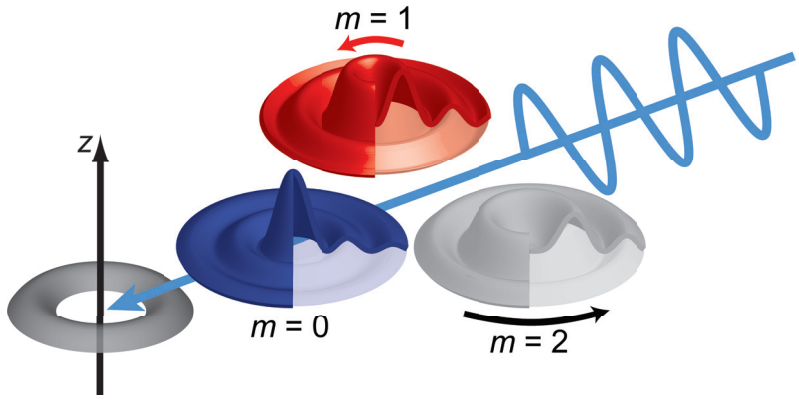

Figure 3.3. Schematic representation of the decomposition of the plane wave to the OAM eigenmodes of light. In here, only the m-modes carrying 0, $\hbar$ and $2\hbar$ of OAM are shown from the infinite number of OAM modes included in the plane wave. The intensity profiles (blue, read and gray objects) depend on the angle between the light propagation direction and the OAM measurement axis z (that is also the symmetry axis of the QR). The overlapping of the intensity profile and QR defines directly the magnitude of effects related to the particular m mode.

OAM of carrier states in QRs, as predicted in Publication II?

In general, light modes carrying OAM of $\hbar m$ respect to the z axis of the coordinate system should have a $\mathrm{e}^{\mathrm{i}m\varphi}$ azimuth-angle dependence, as verified in multiple research articles [81–87]. The question above can be answered by using the Jacobi-Anger expansion for a plane-wave:

$$\mathrm{e}^{\mathrm{i}\mathbf{q}\cdot\mathbf{r}} = \mathrm{e}^{\mathrm{i}q_z z} \sum_{m=-\infty}^{\infty} \mathrm{i}^m J_m(q_\parallel \rho)\mathrm{e}^{\mathrm{i}m(\varphi-\varphi_q)}, \tag{3.1}$$

where J_m is the Bessel function of the first kind of the order of m, φ_q defines the azimuth angle of the propagation direction and $q_\parallel$ ($q_\perp$) is the QR-plane (z-directional) component of the wave vector shown in Fig. 3.1(a). Here the needed $\mathrm{e}^{\mathrm{i}l\varphi}$ phase dependence is found. This expansion shows that a plane wave is actually a superposition of infinitely many OAM eigenmodes of light whenever OAM with respect to some other axis than the propagation direction is considered. If OAM is considered with respect to the propagation direction of a plane wave, it is the $m = 0$ eigenmode that cannot induce OAM changing transitions as also shown in Publication II.

The decomposition of a plane wave to the OAM modes with respect to the symmetry axis of QR is schematically shown in Fig. 3.3. One important feature with the decomposition is the shown squared spatial intensity variations of the OAM modes originating mathematically from the Bessel functions. By changing the angle θ, one can change this spatial

dependence as formulated in Eq. (3.1). The interaction strength of each mode with respect to the carrier states of QR is directly defined by overlapping of the particular m light-mode intensity profile and QR structure. For thin enough structures where the radial confinement of SP states is considerably smaller than the wavelength of the field, the spatial overlapping between the Bessel modes and QR can be approximated by $J_m(qR\sin\theta)$. In sufficiently large QRs, one should be able to match the minimum regions of the intensity profiles depicted in Fig. 3.3 by changing the angle θ, and consequently suppress the interaction of the desired mode and QR; or similarly maximize the effects of wanted OAM changing transitions. It has to be noted, that based on the properties of the Bessel functions, one cannot separate effects between transitions with equal $|m|$ in the studied systems. Furthermore, to get pronounced effects for OAM changing transitions, qR should be large enough, as discussed in Publication II and IV.

3.4 Absorption of orbital angular momentum

To demonstrate effects that can be caused by the previously described OAM changing interband transitions, angle-of-incidence-dependent absorption for a QR system was solved in Publication II. This was done in the low-density regime of carriers by solving the semiconductor Bloch equation for microscopic polarization [14]. The obtained polarization equation was used to formulate absorption $\alpha(\theta,\omega)$ for a plane-wave light field at ω frequency propagating at angle θ with respect to the axis of QR. The found Elliott formula for absorption can be given by

$$\alpha(\theta,\omega) = |d_{c,v}|^2\gamma\sum_{M,\nu}\frac{|\mathcal{F}_{M,\nu}|^2 J_M^2(Rq_\omega\sin\theta)}{(\mathcal{E}_{M,\nu}-\hbar\omega)^2+\gamma^2}, \tag{3.2}$$

where q_ω is the length of vector $\mathbf{q}$ related to the frequency ω. In the given equation, the approximation of an infinitely thin QR structure has been used for DMEs, which is justified whenever the wavelength of the light field is much longer than the spreading of ρ-z plane confinement functions. The dephasing factor γ includes the contribution of otherwise omitted doublets that will lead to the exciton induced dephasing of interband polarization [17]. The broadening of the resonances caused by γ can be also used to describe different scattering processes in the system, size distribution of QRs, if an ensemble of QRs is measured, and even asymmetries in QR structures [17, 53].

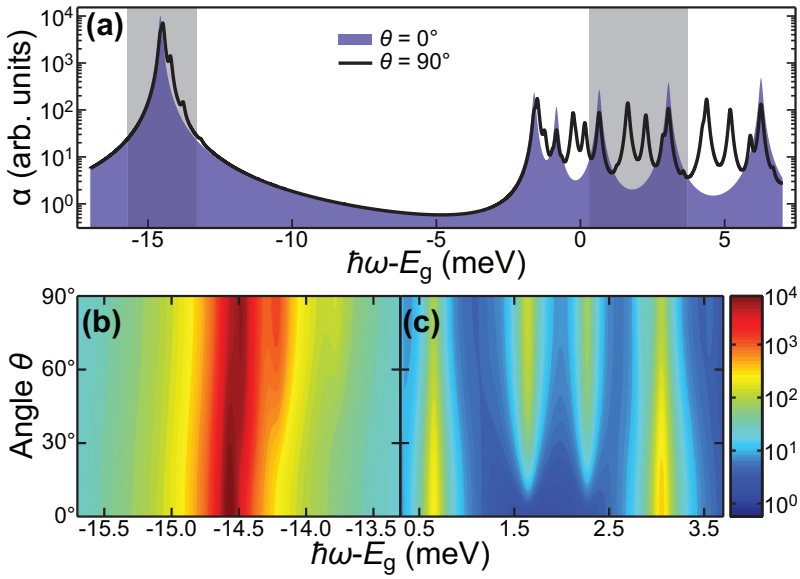

Figure 3.4. Angle-of-incidence θ dependent absorption in a QR system. (a) The absorption spectra obtained with a plane wave propagating either parallel (blue area) or perpendicular (black line) to the QR symmetry axis show pronounced differences. The regions of interest shown in (b) and (c) are indicated by the shaded areas. (b) For the $1s$ resonances the angular dependence is not so pronounced as within the quasicontinuum region (c) where energy separations between resonances are much larger.

Figure 3.4 shows the absorption resulting from Eq. (3.2) with $\gamma = 60$ μeV for the model QR system near the band gap. In Fig. 3.4(a), the overall features of absorption are shown for the two angles $\theta = 0°$ (blue area) and $\theta = 90°$ (black line) with pronounced differences. With the angle $\theta = 0°$ no OAM changing transitions occur; as a result all the resonances can be connected to the $M = 0$ excitonic states. However, when the angle is changed to $90°$ the $M = 0$ resonances are weakened and new peaks emerge, as most clearly seen in the quasicontinuum region where $\hbar\omega > E_g$. The new peaks are resulting from the absorption given by the $M \neq 0$ excitonic states.

In addition to illustrating that the absorption is dependent on the angle θ, Fig. 3.4 also depicts many results based on the properties of excitonic states already discussed in Section 3.2. For example, the difference of the oscillatory strengths between $1s$ excitons (near $\hbar\omega - E_g = -15$ meV) and ionized solutions ($\hbar\omega > E_g$) results in one order of magnitude stronger resonances for the $1s$ states. Also the difficulty of separating $1s$ states with different M values from the resonances of the spectrum is illustrated. Only minor variations related to different energies of $(M, 1s)$ excitons are

found near the ground-state resonance in absorption spectrum for $\theta = 90°$. This region of interest is also plotted in Fig. 3.4(b), where the minor change of the strongest resonance location from $\hbar\omega - E_g = -14.6$ meV to $\hbar\omega - E_g = -14.5$ meV is found when the angle of incidence is increased from $0°$ to $90°$. This variation in the peak position is related to the shift of the strongest $1s$ resonance from $M = 0$ to $M = \pm 1$.

Even these small variations in spectra near the ground-state resonance would vanish if the used dephasing factor would be only slightly larger than the used $\gamma = 60$ μeV, which already gives the linewidth that is near the smallest ones measured in single QR photoluminescence experiments [68]. In the region of large γ values, one interesting additional result arises. In this region where $(\mathcal{E}_{M,1s} - \hbar\omega)^2 \ll \gamma^2$, the frequency dependence near bright $1s$ resonances can be removed from Eq. (3.2). Since the related oscillatory strengths for $1s$ states are M independent, as described in Sec. 3.2, the absorption becomes approximately dependent only on the sum of Bessel functions, $\sum_M J_M^2(Rq\sin\theta)$. Because this sum fulfils the identity

$$\sum_{M=-\infty}^{\infty} J_M^2(x) = 1 \tag{3.3}$$

for any argument value x, it follows that the absorption of $1s$ states becomes approximately θ independent, for sufficiently large γ.

Similar spectral resolution restrictions do not hold for the quasicontinuum region of ionized solutions where the excitonic energies are mostly dependent on SP properties. In Fig. 3.4(c), typical energy separations of millielectronvolt magnitude can be found between $M = 0$ and $M = \pm 1$ resonances. These energy separations are increased when one moves toward higher energy values. In a realizable QR system with suitable materials and geometry, energy separations between bright $M = 0$ and $M = \pm 1$ ionized excitonic solutions can be expected to approach even the range of 10 meV.

It should be noted that these resonances cannot be taken as an evidence for the existence of exciton populations as no carrier populations are involved. Even though there would be carriers present, the absorption in Eq. (3.2) can be used to test where the light induced electronic transitions are most pronounced [17]. However, from the behavior of excitonic resonances one can deduce that the related excitons can be created at corresponding frequency by selecting the correct angle of incidence. This holds also for the $1s$ states, where one usually loses the frequency dependence,

while the angle dependent features are still present. As a result, it should be possible to excite excitons with different OAM values in a controlled manner even with a plane-wave field by changing the angle of incidence. How the obtained OAM dependent distribution of excitons could be detected is discussed in the next section. Since the angular momentum of the whole system is a conserved quantity, the presented results suggest that by altering the angle of incidence and by producing rotating carrier excitations to the ring, one is able to "harvest" OAM components from the plane waves with QRs.

3.5 Emission from rotating excitons

In addition to solving the angle-of-incidence-dependent absorption, the influence of the OAM changing transitions to the PL from QRs were also studied. To model the spontaneous emission from a QR structure, one needs to study the properties of the quantized light field in Eq. (2.4) instead of the classical approach used in the previous section [15]. In more detail, the dynamics of photon correlation $\Delta\langle B^{\dagger}_{q_{\parallel}} B_{q_{\parallel}}\rangle$, which is equal to the expectation value of photon-number operator $\langle B^{\dagger}_{q_{\parallel}} B_{q_{\parallel}}\rangle$ in the incoherent regime [15], is solved in Publication III. In this article, the semiconductor luminescence equations [17] were formulated for arbitrary quantum structures and for arbitrary light modes. These luminescence equations were used in Publication IV to give the steady-state Elliott luminescence formula [15] for QRs

$$I_{\mathrm{PL}}(\theta,\omega) = 2|d_{c,v}|^2\gamma\frac{\mathrm{E}_{\omega}^2}{\mathcal{V}\hbar}\sum_{M,\nu}\frac{|\mathcal{F}_{M,\nu}|^2 J_M^2(Rq_{\omega}\sin\theta)(\Delta N_{M,\nu}+N^S_{M,\nu})}{(\mathcal{E}_{M,\nu}-\hbar\omega)^2+\gamma^2}, \quad (3.4)$$

which gives the PL intensity $I_{\mathrm{PL}}(\theta,\omega)$ for a plane-wave mode with frequency ω and that propagates at an angle θ with respect to the axis of QR. In Eq. (3.4), the dephasing factor γ has many connections to the dephasing factor in the Elliott formula (3.2) for absorption, even though its explicit origin emerges from the phenomenological description of otherwise omitted triplet terms [15].

Equation (3.4) has basically the same form as Eg. (3.2), but in here the important terms $\Delta N_{M,\nu}$ and $N^S_{M,\nu}$ appear, which are the exciton density and the corresponding plasma contribution to PL, respectively [15]. In general, these terms can prevent the use of the Bessel function identity in Eq. (3.3) regardless of the magnitude of γ. Thus, it should be possible to obtain different PL results for different θ angles even with considerably

large γ. Especially, if contributions $\Delta N_{M,\nu}$ and $N^S_{M,\nu}$ are different enough for different M channels.

In the low-density regime of carriers, studied in Publication IV, PL given by Eq. (3.4) is highly sensitive to exciton densities and only minor contribution follows from the $N^S_{M,\nu}$ part [15]. Furthermore, if one focuses on the PL given by the $1s$-like excitons, the related plasma parts, $N^S_{M,1s}$, can be proven to be approximately equal for different M values. This is based on the similarity of the $1s$ wave functions of different M channels and the resulting carrier occupations for exciton densities $\Delta N_{M,1s}$, which can be calculated consistently by following the conservation rules given in Ref. [88]. As a result, the Bessel function identity in Eq. (3.3) can be applied for the plasma contribution of PL when γ is large enough. Consequently, the plasma PL does not show θ dependence for systems with high enough dephasing. Similar results can be expected if the exciton densities for different M channels are approximately the same. This kind of situation can be obtained, for example, with thermal distribution of excitons, in a large enough QRs where the energy separation between $1s$ excitons are small compared to the temperature of the exciton distribution.

In Fig. 3.5, the main results of Publication IV are represented. Figure 3.5(a) illustrates PL from the thermal distribution of excitons with small $\gamma = 60$ μeV for two different angles $\theta = 0^\circ$ (shaded area) and $\theta = 90^\circ$ (black line). The found PL spectra near $1s$ resonances have almost exactly the same characters as the absorption in the same energy range. With angle $\theta = 0^\circ$ the resonance can be directly connected to the $M = 0$ ground-state exciton of the thermal distribution, whereas with $\theta = 90^\circ$ its strength has reduced while the $M = \pm 1$ bound $1s$ states provide the strongest peak, and also the resonance from $M = \pm 2$ is clearly visible near $\hbar\omega - E_g = -14.2$.

To study how strong the angle-of-emission dependence for different excitation conditions are, one can calculate the relative emissions between some angle θ and PL given parallel to the symmetry axis of the ring:

$$\Delta\mathrm{PL}(\theta,\omega,\gamma) = \frac{I_{\mathrm{PL}}(\theta,\omega,\gamma) - I_{\mathrm{PL}}(0^\circ,\omega,\gamma)}{I_{\mathrm{PL}}(\theta,\omega,\gamma) + I_{\mathrm{PL}}(0^\circ,\omega,\gamma)}, \tag{3.5}$$

where the γ dependency of PL is now denoted explicitly. In Fig. 3.5(b), the relative PL is shown for four different excitation conditions for a relatively large $\gamma = 1$ meV with frequency ω that corresponds to the energy of the ground-states exciton. As discussed earlier, it is found that the thermal contribution at 30 K temperature (dashed grey line) does not show basically any angular dependence. However, the excitations where only

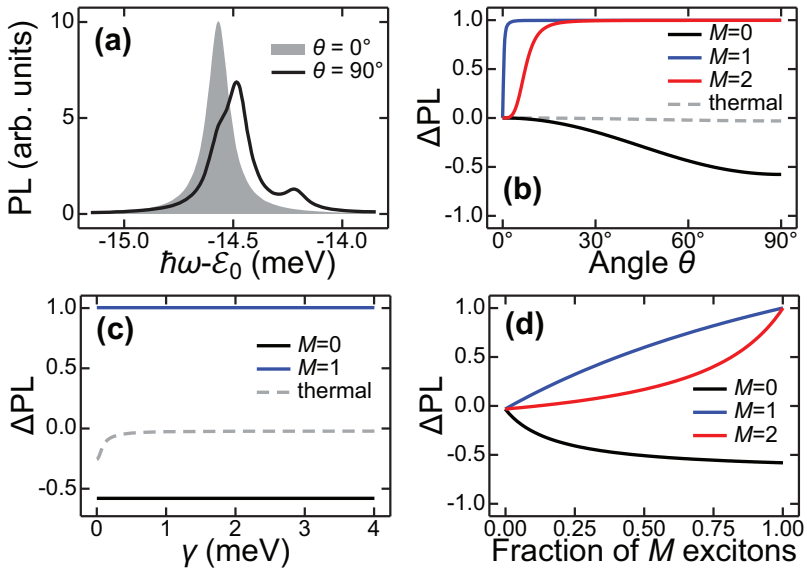

Figure 3.5. Angle-of-emission dependent QR luminescence. (a) With high enough temperatures and small enough γ, the PL resonances connected to different M channels can be separated from spectra, as illustrated for the angles $\theta = 0°$ (shaded area) and $\theta = 90°$ (black line). (b) When broadening of resonances is larger than the frequency-domain separability of $1s$ states, the thermal distribution (dashed gray line) does not show angle dependence, whereas the excitations including only $M = 0$ (black line), $M = 1$ (blue line) or $M = 2$ (red line) $1s$ excitons show pronounced dependence on angle-of-emission θ. (c) The angular dependence is not dependent on the magnitude of dephasing factor γ for distributions that have only $M = 0$ (black line) or $M = 1$ (blue line) $1s$ excitons. For small γ values, the thermal distribution (dashed gray line) shows γ dependence that is related to the frequency-domain separability of exciton resonances shown in (a). (d) The added $M = 0$ (black line) or $M = 1$ (blue line) excitons can be detected from the thermal background distribution even with small fractions of added M states respect to the total number of excitons in the system. Clearly observable effect for additional $M = 2$ (red line) excitons needs much higher fractions.

one type of $1s$ excitons is present: $M = 0$ (black line), $M = 1$ (blue line) or $M = 2$ (red line), a pronounced θ dependence can be found. This suggests that the distribution of different M excitons could be determined by measuring the angle dependent PL.

In Fig. 3.5(c), the γ dependence of $\Delta\mathrm{PL}(90°, \omega, \gamma)$ is depicted, now with respect to ω that corresponds to the peak frequency at angle $\theta = 90°$. The thermal distribution of excitons (dashed grey line) shows γ dependence for small enough dephasing factor values, resulting from the frequency-domain separability of resonances illustrated in Fig. 3.5(a). However, when the line broadening, given by γ, exceeds the separability of $M = 0$ and $M = \pm 1$ resonances near $\gamma = 0.3$ meV, the angular dependence of thermal distribution is lost. In contrast, the angular dependence of exci-

tations with only one type of M excitons show no γ dependence, as illustrated for $M = 0$ (black line) and $M = 1$ (blue line) excitations.

In a realistic situation, it cannot be assumed that one could have an excitation where only one type of M excitons would appear. It can be expected that the different scattering processes, e.g. ones related to phonons or structure asymmetries, will distribute excitons to different M channels. To study how well different explicit M excitons could be detected from such distributions, the relative PL from a mixture of thermal distribution (at 30 K) and an additional M exciton were calculated. Figure 3.5(d) shows these results as a function of a fraction of additional $\Delta N_{M,1s}$ with respect to the total density of excitons. The figure illustrates that the additional $M = 0$ (black line) and $M = 1$ distributions lead to pronounced angle-dependence even with quite small fractions of added excitons, whereas the $M = 2$ (red line) contribution is not so easily detectable. In Publication IV, it was also shown that if a larger radius QR is used, it is possible to detect $1s$ states with much higher M numbers from the thermal background. In general, the angle-resolved PL results presented here suggest that PL is a suitable way to detect different M channels of excitons. This, in turn, would lead to the possibility of studying fundamental properties of light–matter OAM coupling in the microscopic level, when also the excitation of these excitons via absorption is considered.

4. Coherent control of spatial distribution of excitations in quantum-well structures

Controlling the movement of carriers in semiconductor systems is highly important field of study. Basically, the operational principles of most semiconductor devices are more or less based on the transfer properties of electrons and holes [89, 90]. In this field, one important branch of study is the research on vertical transport through material interfaces. A high number of important applications including quantum cascade lasers [16, 91, 92], tunnel-junction devices [13] and solar cells [6, 7] directly involve transport of carriers or other excitations through semiconductor interfaces.

To study the vertical transport through interfaces, it would be beneficial to have coherent-control schemes where one could be able to control the transport of different types of excitations with varying characteristics. Consequently, one should be able to use this transfer scheme to reveal fundamental properties of the vertical excitation transport. One possible set-up for studying the transport effects could include a semiconductor structure of planar heterojunctions, i.e. a multi-QW structure. Within these systems, different types of excitation conditions can be initialized with a controllable manner by optical fields [17]. With optical fields, one can excite different types of semiconductor quasiparticles like electron–hole plasma, excitons, biexcitons, and even massive quasiparticles like dropletons [93] into QWs. Simultaneously as transporting different quasiparticles, one is able to transport also related quantum mechanical quantities like spins or correlations, which for different types of particles can have considerably different physical behavior. As the transition energies between quasiparticles in a same group are typically in the range of a few meV [15], the electrical THz fields should be a suitable tool to achieve desired transitions.

In this thesis, a double QW with real-space type-I and type-II properties of semiconductor system [14] is taken as a model structure for studying THz coherent-control schemes of quasiparticle transport. In this structure, the holes are confined to one of the wells while electrons can be transported through an interface separating the QW regions. Similar structures have been realized with multiple different material combinations, applied for practical applications, like W-lasers, and even used to demonstrate possibilities for observing Bose-Einstein condensates of excitons [94–97]. Even though the detailed knowledge on the physical properties of these structures, especially on truly microscopic level, is not so well understood as in more conventional QWs, there are still numerous theoretical studies in this field [98–101].

In this chapter, an idea of coherent-control scheme of transporting quasiparticles through semiconductor interfaces with THz pulses is presented. The plausibility of the idea is studied in the model structure where it is shown that a highly efficient and selective transport of either free or exciton bound electrons is achievable in a realizable system. At the end, based on the high selectivity of found electron- and exciton-transport protocols, a novel transport scheme where only excitonic correlations are transported is presented.

4.1 The idea of THz coherent control of vertical quasiparticle transport

As already discussed, the typical transition frequencies between excitations inside different semiconductor quasiparticle groups are in the THz range. As a result, it should be possible to induce transitions between similar quasiparticles by applying suitable THz pulses. This has been experimentally demonstrated between excitons in the same QW by introducing transitions between $1s$ and $2p$ excitons [102]. Similarly, THz induced transitions between confinement levels of electrons inside a QW have been observed [103].

By generalizing these results for multi-QW structures, it should be possible to induce transitions between quasiparticle states in different QWs with a similar approach as used in Ref. [103] by applying a THz field, which is polarized so that its electric field has a component parallel to the structure growth direction. As in this case, the confinement functions of electrons in different subbands can be predominantly located in different

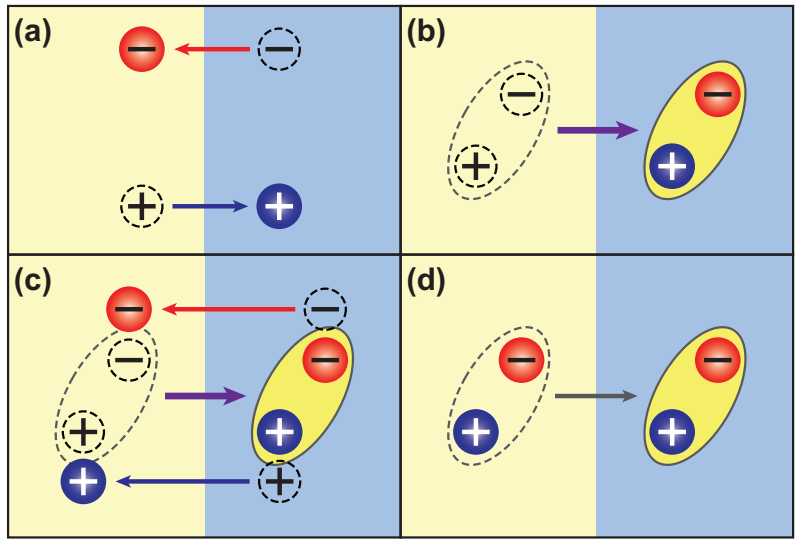

Figure 4.1. Idea of coherent control of vertical transport of quasiparticles. (a) When the frequency of field inducing transports is tuned to match the difference of electron or hole transition energies, electrons (red spheres) or holes (blue spheres) can be transported between materials (yellow and blue areas). (b) Exciton transport is obtained by using the field frequency corresponding to exciton transition energy. (c) If the different transport protocols for electrons, holes and excitons are selective enough, they can be applied simultaneously to transport SP states and correlated pairs to opposite direction. As no net transport of carriers is obtained in this case, the transport only transfers exciton correlations as summarized in (d).

spatial regions of the structures, quasiparticle transitions will also lead to spatial transport of particles. Furthermore, if the transition frequencies for different quasiparticles are distinct enough, this should also introduce a coherent-control scheme where one is able to selectively transport only wanted excitations. This idea is illustrated in Fig. 4.1 for a system where only electrons (red spheres), holes (blue spheres) and exciton correlations (yellow ellipses) are considered. In this figure, the initial states before transport are depicted by dashed-line objects while the transport phenomena themselves are shown by arrows.

In the first case illustrated in Fig. 4.1(a), the THz field is tuned to correspond to the transition frequency of electrons or holes between the different material regions (yellow and blue areas). In this case, only uncorrelated carriers are moved. In the next case depicted in Fig. 4.1(b), the THz frequency matches exciton transition, which causes the transport of a correlated electron–hole pair. If these singlet- and doublet-transport protocols in Figs. 4.1(a) and (b), respectively, are selective enough, one can simultaneously transport electrons and holes as well as excitons to

desired direction, as shown in Fig. 4.1(c). The possibility of this type of control is directly related to the difference of transition energies that need to be large enough compared to the broadening of the transfer resonances, which is eventually related to the scattering and dephasing processes in the system [17]. If high enough selectivity for the different transports is achieved, it is possible to obtain transport processes where the single particle densities remain constant as schematically shown in Fig. 4.1(d), which summarizes the net effect of transport phenomena in Fig. 4.1(c). In this case, one effectively transports only quantum mechanical properties related to quasiparticles, like correlations, instead of transporting actual carriers.

4.2 Properties of electron–hole pairs in model double-QW structure

The plausibility of the ideas introduced in the previous section is studied in Publication V. In this article, a double-QW structure, where the hole is always in one well while the electrons can be transported, is selected as a model system. This provides a simpler scheme than the one illustrated in Fig. 4.1, as one needs only to consider transport of electrons or the electronic part of excitons. Furthermore, in this system the thicknesses of the quantum wells are chosen to be so thin that it is sufficient to study two energetically lowest confinement levels of electrons and the confinement ground level of holes, to model electron and exciton transports. The system is GaAs based where the left QW potential, corresponding to type-I configuration, is produced by InGaAsN compound. The QW providing the type-II spatial configuration for electrons and holes is fabricated from a GaAsN while the barrier and buffer material is GaAs. The schematics of band edges giving the confinement potentials are shown in Fig. 4.2 and details of the structure are given in the supplemental material of Publication V.

The modeling of the double-QW system is started from the SP level, where the electronic wave functions in the envelope-function approximation are solved from Eq. (2.2). As a result, the energy separation between the considered electron confinement subbands, shown in Fig. 4.2 by red shapes, is found to be given by the transition energy of 20 meV. This energy corresponds to the frequency $\nu_{\mathrm{e}} = 4.8$ THz. To characterize the properties of excitons, the Coulomb matrix elements for the structure are calculated from Eq. (2.8) and the corresponding low-density Wannier

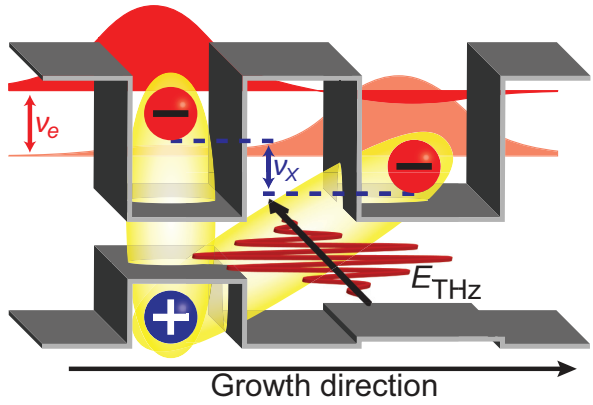

Figure 4.2. Schematics of the model double-QW system. The conduction- and valence-band profile (grey structure) confines electrons (red spheres) to two relevant confinement levels (red areas) located in the different wells, and holes (blue sphere) only to the left QW. In this system, THz field (red wave symbol with black arrow) can induce transport of electrons from well to well, by transporting either plasma electrons with frequency ν_e or electrons confined to excitons (yellow ellipses) with frequency ν_X.

equation (2.14) is solved. Following from the spatial separation between electrons and holes located in different QWs compared to the electrons in the same well as the holes, the CMEs between the holes and indirect electrons are much smaller than the corresponding matrix elements for the direct electrons. As a straightforward consequence, the binding energy of 4.73 meV for indirect $1s$ exciton is found to be considerably smaller than the binding energy of 9.83 meV of the direct $1s$ state. As a result, the transition energy between direct and indirect $1s$ state is not directly given by the electronic confinement energies and is found to equal 14.90 meV that corresponds to the transition frequency ν_X = 3.6 THz. Both characteristic transition frequencies, the electronic ν_{e} and excitonic ν_{X}, are schematically illustrated in Fig. 4.2.

As the transition energies between uncorrelated and exciton correlated electrons are substantially different, it can be assumed that in the studied system, selective transport of electrons or excitons can be achieved. This can be done if the transport resonances are not too wide so that they would drastically overlap. In the studied system where the energetic separation between electron and exciton transport is 5.1 meV, this could be roughly obtained if the dephasing times of intersubband correlations involved in the transitions will be longer than 500 fs, which approximately correspond to 3 meV homogeneous broadening of transport resonances. This limit is achievable in high quality QWs that resemble the model structure, as

dephasing times up to 7 ps have been reported in these systems [104].

4.3 Correlation transport

In order to more explicitly study how well the selective transport protocols of electrons and excitons can be utilized in the model system, one needs to solve the dynamics for the electron and exciton densities. A closed set of singlet-doublet equations is formulated between electron and hole occupation numbers as well as for the excitonic correlations and intersubband polarizations. This is done by applying the cluster-expansion approach together with the main-sum approximation, which is valid in the studied low-density regime of carrier densities [15, 17].

The THz field that is inducing transitions, was selected to propagate in the structure plane with electrical field polarized to the growth direction, as Fig. 4.2 illustrates with the black arrow and the red wave symbol. The used field polarization was selected to ensure the strongest possible transport effect and to conserve the symmetry of initial excitons, which are assumed to be produced by optical excitation leading dominantly to s-like states [17]. As a result, the relevant dipole elements for the electron-electron intersubband transitions are given by Eq. (2.13). Furthermore, the used THz pulses were assumed to have Gaussian envelope with duration in the picosecond scale.

By utilizing different dephasing times between relevant quasiparticles and coherences [17], a diffusive dephasing model was introduced. In this model, the total quasiparticle densities for electrons, holes and excitons were taken to be constant during the picosecond time scale under interest while all other quantities were dephased. These quantities involve intersubband polarizations and correlated exciton transition amplitudes [17]. For both of these intersubband coherences a dephasing time of 1.3 ps was selected. All interband coherences were assumed to be vanished after initial optical excitation.

After formulating the explicit dynamical equations, calculations were made to verify the selectivity and efficiency of electron and exciton transports. This was done for two initial states where all electrons were either as plasma or bound to $1s$ excitons. In both cases, all electrons were initially in the indirect (right) QW. The maximum fraction of transported electrons from right to left was studied as a function of THz frequency and intensity of the pulse. As predicted, a clear maximum for plasma trans-

fer was obtained when the frequency of THz pulse matched $\nu_{\mathrm{e}} = 4.8$ THz. Similarly, in the exciton bound case, the electrons were transported most efficiently with ν_X = 3.6 THz. Furthermore, the obtained results could be used to define the efficiency and selectivity of the electron- (ν_e) and exciton-transport (ν_X) protocols. The efficiency of 80% was found for both protocols, which defines the maximal fraction of transported electrons in plasma or exciton bound cases. The selectivity of 95% was found to be equal for both protocols. In here, the selectivity describes how large fraction of transported electrons are either free or correlated with respect to desired results; i.e. electron-transport protocol transfer twenty times more free electrons than correlated ones. The reduction of both, efficiency and selectivity, from their ideal values of 100% is mostly caused by the used dephasing model.

Figure 4.3(a) illustrates the electron- and exciton-transport protocols, in a case where all initial electrons are in the right (R) QW. In here, fractions of 65% of plasma electrons and 35% of indirect $1s$ bound electrons are selected. Two sequential pulses are applied to the system as depicted in Figure 4.3(a-i). The first pulse is the electron-transport pulse at frequency ν_e. As seen from Figure 4.3(a-ii), it transports roughly half of the electron density to the left (L) QW while the correlations in Figure 4.3(a-iii) remain almost intact. This demonstrates the high selectivity of the plasma protocol. During the second pulse at frequency ν_e, the remaining electrons in the right QW are transported to the left, as seen from Figure 4.3(a-ii). This time also correlations are transferred as illustrated by Fig. 4.3(a-iii). As a result, one can conclude that excitons were transported.

As the studied electron- and exciton-transport protocols were found to be highly efficient and selective, even in the presence of the realistic contribution of dephasing, one can also study if the coherent control of exciton-correlation transport, as illustrated in Fig. 4.1(d) for a more general system, is also achievable in the model structure. The results obtained in Publication V are presented in Fig. 4.3(b), where the same initial state of the system is assumed as in the previous case. The applied pulses are shown in Fig. 4.3(b-i), where the first pulse is again the electron-transport protocol that separates the correlated and uncorrelated electrons to different QWs. This time, the second pulse is a two-color, super-position pulse that includes both frequency components, ν_e and ν_X. The transport results obtained during the second pulse drastically differ from the exciton-transport protocol studied previously. Also this time the correlations are

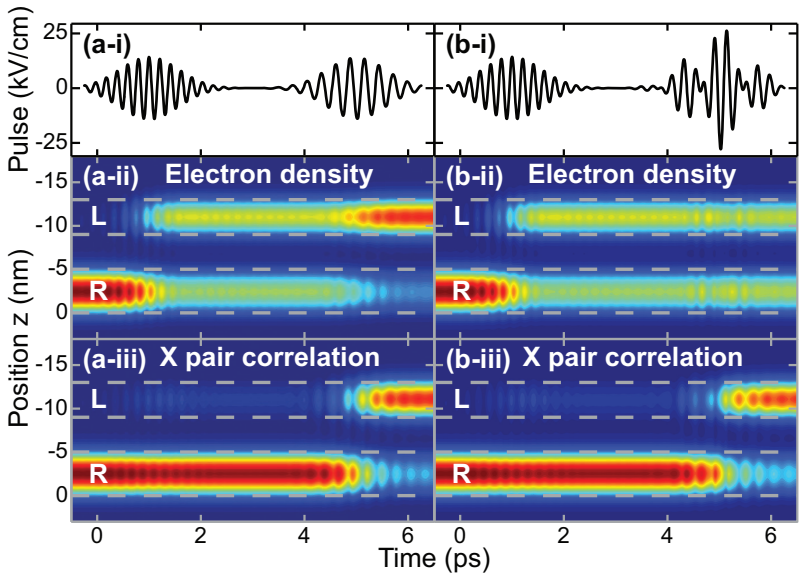

Figure 4.3. Demonstration of coherent control of electron, exciton and correlation transport. (a) Two sequential pulses with frequencies ν_e and ν_X are applied to the system. The first pulse transports uncorrelated electrons while the second one moves correlated ones, as depicted by (a-ii) and (a-iii). (b) The correlation-transport protocol is achieved via the second pulse that includes both frequency components ν_e and ν_X. As seen form (b-ii) and (b-iii), during this pulse correlations are moved while electron densities remain almost constant.

transported from right to left, as Fig. 4.3(b-iii) depicts, but now the electron densities in Fig. 4.3(b-ii) remain essentially constant. Consequently, only the quantum correlations have been transported and the possibility to obtain a new method to coherently control the transport of purely quantum-mechanical properties is demonstrated. This effect has many similarities with the coherently controlled spin currents, where continuous flow of spin is achieved instead of transporting correlations [105, 106].

5. Conclusions and outlook

In this thesis, theoretical microscopic models describing single-particle states and many-body physics of semiconductor quantum-ring structures is formulated. These models have been used to characterize the properties of electron, hole and exciton states in QRs. The light–matter coupling in the submicron ring structures is studied for classical and quantum optical fields. Based on the microscopic many-body models, the results are presented for absorption and emission of light for the QR system. Both of these results indicate a strong angular dependence on the angle between the QR symmetry axis and the propagation direction of light. The angular dependence has a profound connection to the coupling of orbital angular momentum between light and quasiparticles. It was found that the plane waves can excite excitons with various OAM quantum numbers, and it is proposed that the distribution of OAM between excitons can be measured and used to verify the light–matter OAM coupling via PL.

The second main theme of the thesis is the coherent control in the THz range of vertical quasiparticle transport through internal interface of a semiconductor heterojunction. In here, it was verified by microscopical modeling that such a transport scheme exists in a realizable double-QW structure. In the model structure, highly selective electron-, exciton- and correlation-transport protocols have been devised. This kind of coherent control scheme is a novel idea. Especially, the correlation-transport effect is something that has not been previously reported and provides a new method to create currents with quantum mechanical properties.

One combining feature between the two study branches is that the obtained results are not just restricted to the numerically modeled cases, but they predict new fundamental physical effects that are not dependent on exact geometry and material parameters. As a consequence, the most important step for further studies involving the presented results

should be the verification of introduced effects in experimental measurements. There are naturally also additional theoretical aspects related to this work that should be further studied. For example, the inclusion of phonons to the QR should be done to give time scales and fundamental understanding on the coherence times of OAM excitons in QR systems. Similar studies are also important for the double-QW structure, where the phonon induced relaxation processes between the wells are important. Also the inclusion of multiple electron and hole confinement levels to the THz coherent-control scheme would be beneficial for modeling more complicated designs.

In addition, the found-quantum mechanical effects are not only of academic interest. It has been shown that both the orbital angular momentum of light and THz fields, are highly efficient in information technologies. By utilizing these characters of optical fields, records for the data-transport rates have been reached [107, 108]. Furthermore, OAM of light has been proven to be one of the most promising approaches in quantum information technology [81, 109, 110]. The coupling between OAM of light and matter in a microscopic level has gained considerable interest, based on the opportunities it could provide for quantum technologies [81, 110]. So far, single-atom experiments with OAM of light have not been published while the OAM interaction between light and ensembles of atoms have been observed [111–115]. In this field, the presented results of the coupling between single excitonic states of QRs can lead to new approaches in the future. Even the obtained result for correlation transport, presented in this thesis, can provide to be important in quantum technology, as the correlations are tightly related to the non-locality of quantum mechanics and to such phenomena as entanglement. However, the most prominent field to apply the obtained results for multi-QW structures is the characterization of fundamental properties of transport effects. This could be used to optimize and improve the performance of already existing devices, and of course to develop novel systems where the coherent control of semiconductor quasiparticle transport can be utilized.

Bibliography

[1] L. L. Chang, L. Esaki, R. Tsu, *Appl. Phys. Lett.* **24**, 593 (1974).

[2] R. Dingle, W. Wiegmann, C. H. Henry, *Phys. Rev. Lett.* **33**, 827 (1974).

[3] Y. Arakawa, A. Yariv, *IEEE J. Quantum Electron.* **22**, 1887 (1986).

[4] M. H. Huang, *et al.*, *Science* **292**, 1897 (2001).

[5] V. I. Klimov, *et al.*, *Science* **290**, 314 (2000).

[6] R. Dahal, B. Pantha, J. Li, J. Y. Lin, H. X. Jiang, *Appl. Phys. Lett.* **94**, 063505 (2009).

[7] P. V. Kamat, *Acc. Chem. Res.* **45**, 1906 (2012).

[8] S. Zimmermann, A. Wixforth, J. P. Kotthaus, W. Wegscheider, M. Bichler, *Science* **283**, 1292 (1999).

[9] M. Kroutvar, *et al.*, *Nature* **432**, 81 (2004).

[10] M. Geller, *et al.*, *Appl. Phys. Lett.* **92**, 092108 (2008).

[11] D. L. Klein, R. Roth, A. K. L. Lim, A. P. Alivisatos, P. L. McEuen, *Nature* **389**, 699 (1997).

[12] R. J. Warburton, *et al.*, *Nature* **405**, 926 (2000).

[13] J. P. Pekola, *et al.*, *Rev. Mod. Phys.* **85**, 1421 (2013).

[14] H. Haug, S. W. Koch, *Quantum Theory of the Optical and Electronic Properties of Semiconductors* (World Scientific Publishing, Singapore, 2009), fifth edn.

[15] M. Kira, S. W. Koch, *Semiconductor Quantum Optics* (Cambridge University Press, Cambridge, 2011).

[16] J. Faist, *et al.*, *Science* **264**, 553 (1994).

[17] M. Kira, S. W. Koch, *Prog. Quantum Electron.* **30**, 155 (2006).

[18] S. W. Koch, M. Kira, G. Khitrova, H. M. Gibbs, *Nat. Mater.* **5**, 523 (2006).

[19] G. Bastard, *Phys. Rev. B* **24**, 5693 (1981).

[20] G. Bastard, *Wave Mechanics Applied to Heterostructures* (Les Editions de Physique, Paris, 1988).

[21] M. G. Burt, *Semicond. Sci. Technol.* **2**, 460 (1987).

[22] M. G. Burt, *J. Phys.: Condens. Matter* **4**, 6651 (1992).

[23] M. G. Burt, *J. Phys.: Condens. Matter* **11**, 53 (1999).

[24] M. F. H. Schuurmans, G. W. 't Hooft, *Phys. Rev. B* **31**, 8041 (1985).

[25] A. T. Meney, B. Gonul, E. P. O'Reilly, *Phys. Rev. B* **50**, 10893 (1994).

[26] B. A. Foreman, *Phys. Rev. B* **72**, 165345 (2005).

[27] E. O. Kane, *Semiconductors and Semimetals*, R. K. Willardson, A. C. Beer, eds. (Academic Press, New York, 1966), vol. 1 of *Semiconductors and Semimetals*, pp. 75–100.

[28] P.-O. Löwdin, *J. Chem. Phys.* **19**, 1396 (1951).

[29] J. W. Matthews, A. E. Blakeslee, *J. Cryst. Growth* **27**, 118 (1974).

[30] E. P. O'Reilly, *Semicond. Sci. Technol.* **4**, 121 (1989).

[31] T. B. Bahder, *Phys. Rev. B* **41**, 11992 (1990).

[32] G. L. Bir, G. E. Pikus, *Symmetry and Strain-induced Effects in Semiconductors* (I.P.S.T., New York, 1975).

[33] E. D. Jones, *et al.*, *Appl. Phys. Lett.* **54**, 2227 (1989).

[34] E. P. O'Reilly, G. P. Witchlow, *Phys. Rev. B* **34**, 6030 (1986).

[35] B. A. Foreman, *Phys. Rev. B* **49**, 1757 (1994).

[36] I. Vurgaftman, J. R. Meyer, L. R. Ram-Mohan, *J. Appl. Phys.* **89**, 5815 (2001).

[37] I. Vurgaftman, J. R. Meyer, *J. Appl. Phys.* **94**, 3675 (2003).

[38] J. D. Joannopoulos, S. G. Johnson, J. N. Winn, R. D. Meade, *Photonic Crystals: Molding the Flow of Light* (Princeton University Press, Princeton, 2008), second edn.

[39] A. Yariv, *Electron. Lett.* **36**, 321 (2000).

[40] Y. Aharonov, D. Bohm, *Phys. Rev.* **115**, 485 (1959).

[41] M. Büttiker, Y. Imry, R. Landauer, *Phys. Lett. A* **96**, 365 (1983).

[42] T. Chakraborty, P. Pietiläinen, *Phys. Rev. B* **50**, 8460 (1994).

[43] A. C. Bleszynski-Jayich, *et al.*, *Science* **326**, 272 (2009).

[44] J. M. Garcia, *et al.*, *Appl. Phys. Lett.* **71**, 2014 (1997).

[45] B. C. Lee, O. Voskoboynikov, C. P. Lee, *Phys. E* **24**, 87 (2004).

[46] T. Kuroda, *et al.*, *Phys. Rev. B* **72**, 205301 (2005).

[47] J. Sormunen, *et al.*, *Nano Lett.* **5**, 1541 (2005).

[48] A. Stemmann, *et al.*, *J. Appl. Phys.* **106**, 064315 (2009).

[49] M. Bayer, *et al.*, *Phys. Rev. Lett.* **90**, 186801 (2003).

[50] B. Hackens, *et al.*, *Nat. Phys.* **2**, 826 (2006).

[51] A. Lorke, *et al.*, *Phys. Rev. Lett.* **84**, 2223 (2000).

[52] R. Römer, M. Raikh, *Phys. Status Solidi B* **221**, 535 (2000).

[53] T. Meier, P. Thomas, S. W. Koch, *Eur. Phys. J. B* **22**, 249 (2001).

[54] A. O. Govorov, S. E. Ulloa, K. Karrai, R. J. Warburton, *Phys. Rev. B* **66**, 081309 (2002).

[55] L. G. G. V. Dias da Silva, S. E. Ulloa, T. V. Shahbazyan, *Phys. Rev. B* **72**, 125327 (2005).

[56] M. D. Teodoro, *et al.*, *Phys. Rev. Lett.* **104**, 086401 (2010).

[57] S.-S. Li, J.-B. Xia, *J. Appl. Phys.* **89**, 3434 (2001).

[58] L. A. Lavenère-Wanderley, A. Bruno-Alfonso, A. Latgé, *J. Phys.: Condens. Matter* **14**, 259 (2002).

[59] S.-S. Li, J.-B. Xia, *J. Appl. Phys.* **91**, 3227 (2002).

[60] O. Voskoboynikov, Y. Li, H.-M. Lu, C.-F. Shih, C. P. Lee, *Phys. Rev. B* **66**, 155306 (2002).

[61] J. Even, S. Loualiche, *J. Phys. A: Math. Gen.* **37**, L289 (2004).

[62] H. Pettersson, *et al.*, *Phys. E* **6**, 510 (2000).

[63] H. Hu, G.-M. Zhang, J.-L. Zhu, J.-J. Xiong, *Phys. Rev. B* **63**, 045320 (2001).

[64] T. Meier, P. Thomas, S. Koch, K. Maschke, *Phys. Status Solidi B* **234**, 283 (2002).

[65] Y. V. Pershin, C. Piermarocchi, *Phys. Rev. B* **72**, 245331 (2005).

[66] D. Granados, J. M. Garcia, *Appl. Phys. Lett.* **82**, 2401 (2003).

[67] T. Raz, D. Ritter, G. Bahir, *Appl. Phys. Lett.* **82**, 1706 (2003).

[68] B. Alén, J. Martínez-Pastor, D. Granados, J. M. García, *Phys. Rev. B* **72**, 155331 (2005).

[69] C. H. Lin, *et al.*, *Appl. Phys. Lett.* **94**, 183101 (2009).

[70] A. V. Maslov, D. S. Citrin, *Phys. Rev. B* **67**, 121304 (2003).

[71] A. M. Fischer, V. L. Campo, M. E. Portnoi, R. A. Römer, *Phys. Rev. Lett.* **102**, 096405 (2009).

[72] G. F. Quinteiro, J. Berakdar, *Opt. Express* **17**, 20465 (2009).

[73] G. F. Quinteiro, A. O. Lucero, P. I. Tamborenea, *J. Phys.: Condens. Matter* **22**, 505802 (2010).

[74] J. A. Barker, R. J. Warburton, E. P. O'Reilly, *Phys. Rev. B* **69**, 035327 (2004).

[75] L. G. G. V. Dias da Silva, S. E. Ulloa, A. O. Govorov, *Phys. Rev. B* **70**, 155318 (2004).

[76] P. Offermans, *et al.*, *Phys. E* **32**, 41 (2006).

[77] V. M. Fomin, *et al.*, *Phys. Rev. B* **76**, 235320 (2007).

[78] S. Viefers, P. Koskinen, P. Singha Deo, M. Manninen, *Phys. E* **21**, 1 (2004).

[79] R. M. Wilcox, *J. Chem. Phys.* **45**, 3312 (1966).

[80] J. Morales, J. Lopez-Bonilla, A. Palma, *J. Math. Phys.* **28**, 1032 (1987).

[81] A. M. Yao, M. J. Padgett, *Adv. Opt. Photonics* **3**, 161 (2011).

[82] L. Allen, M. W. Beijersbergen, R. J. C. Spreeuw, J. P. Woerdman, *Phys. Rev. A* **45**, 8185 (1992).

[83] A. T. O'Neil, I. MacVicar, L. Allen, M. J. Padgett, *Phys. Rev. Lett.* **88**, 053601 (2002).

[84] M. Padgett, J. Courtial, L. Allen, *Phys. Today* **57**, 35 (2004).

[85] G. F. Calvo, A. Picón, E. Bagan, *Phys. Rev. A* **73**, 013805 (2006).

[86] K. Y. Bliokh, M. A. Alonso, E. A. Ostrovskaya, A. Aiello, *Phys. Rev. A* **82**, 063825 (2010).

[87] M. Mansuripur, *Phys. Rev. A* **84**, 033838 (2011).

[88] M. Mootz, M. Kira, S. W. Koch, *New J. Phys.* **15**, 093040 (2013).

[89] D. K. Ferry, S. M. Goodnick, J. Bird, *Transport in Nanostructures* (Cambridge University Press, Cambridge, 2009), second edn.

[90] C. Jacoboni, *Theory of Electron Transport in Semiconductors: A Pathway from Elementary Physics to Nonequilibrium Green Functions* (Springer, Heidelberg, 2010).

[91] R. Köhler, *et al.*, *Nature* **417**, 156 (2002).

[92] B. S. Williams, *Nat. Photonics* **1**, 517 (2007).

[93] A. E. Almand-Hunter, *et al.*, *Nature* **506**, 471 (2014).

[94] K. Hantke, *et al.*, *Phys. Rev. B* **71**, 165320 (2005).

[95] J.-Y. Yeh, *et al.*, *Appl. Phys. Lett.* **88**, 051115 (2006).

[96] M. Motyka, *et al.*, *Appl. Phys. Lett.* **94**, 251901 (2009).

[97] L. V. Butov, A. Zrenner, G. Abstreiter, G. Böhm, G. Weimann, *Phys. Rev. Lett.* **73**, 304 (1994).

[98] J. R. Meyer, C. A. Hoffman, F. J. Bartoli, L. R. Ram-Mohan, *Appl. Phys. Lett.* **67**, 757 (1995).

[99] W. W. Chow, H. C. Schneider, *Appl. Phys. Lett.* **78**, 4100 (2001).

[100] C. Schlichenmaier, S. W. Koch, W. W. Chow, *Appl. Phys. Lett.* **81**, 2944 (2002).

[101] C. Schlichenmaier, *et al.*, *Appl. Phys. Lett.* **86**, 081903 (2005).

[102] W. D. Rice, *et al.*, *Phys. Rev. Lett.* **110**, 137404 (2013).

[103] D. Golde, *et al.*, *Phys. Rev. Lett.* **102**, 127403 (2009).

[104] H. G. Roskos, *et al.*, *Phys. Rev. Lett.* **68**, 2216 (1992).

[105] M. J. Stevens, *et al.*, *Phys. Rev. Lett.* **90**, 136603 (2003).

[106] J. Hübner, *et al.*, *Phys. Rev. Lett.* **90**, 216601 (2003).

[107] J. Wang, *et al.*, *Nat. Photonics* **6**, 488 (2012).

[108] S. Koenig, *et al.*, *Nat. Photonics* **7**, 977 (2013).

[109] A. Mair, A. Vaziri, G. Weihs, A. Zeilinger, *Nature* **412**, 313 (2001).

[110] A. Vaziri, J.-W. Pan, T. Jennewein, G. Weihs, A. Zeilinger, *Phys. Rev. Lett.* **91**, 227902 (2003).

[111] R. Inoue, *et al.*, *Phys. Rev. A* **74**, 053809 (2006).

[112] M. F. Andersen, *et al.*, *Phys. Rev. Lett.* **97**, 170406 (2006).

[113] C. Ryu, *et al.*, *Phys. Rev. Lett.* **99**, 260401 (2007).

[114] Y. Ueno, Y. Toda, S. Adachi, R. Morita, T. Tawara, *Opt. Express* **17**, 20567 (2009).

[115] K. Shigematsu, Y. Toda, K. Yamane, R. Morita, *Jpn. J. Appl. Phys.* **52**, 08JL08 (2013).

Aalto-DD 214/2014

ISBN 978-952-60-6032-3 (printed)
ISBN 978-952-60-6033-0 (pdf)
ISSN-L 1799-4934
ISSN 1799-4934 (printed)
ISSN 1799-4942 (pdf)

Aalto University
School of Electrical Engineering
Department of Micro- and Nanosciences
www.aalto.fi

BUSINESS +
ECONOMY

ART +
DESIGN +
ARCHITECTURE

SCIENCE +
TECHNOLOGY

CROSSOVER

DOCTORAL
DISSERTATIONS